Study of the Ion Kinetic energy distribution in Aluminium using double-laser Pulse Plasma

By

Akhtar Muhammad

Department of Physics

Quaid-i-Azam University

Islamabad, Pakistan

2023

Study of the Ion Kinetic energy distribution in Aluminium using double-laser Pulse Plasma

A dissertation submitted in partial fulfillment of the requirements for the degree of

Master of Philosophy in Physics

by

Akhtar Muhammad

Department of Physics

Quaid-i-Azam University

Islamabad, Pakistan

2023

Certificate

It is certified that the work contain in this thesis is carried out and completed under my supervision at the Atomic and Molecular Physics Laboratory, Department of physics, Quaid i Azam University, Islamabad, Pakistan.

Supervisor:

Raheel Ali

Prof. Dr. Raheel Ali

Atomic and Molecular Laboratory

Department of physics

Quaid-i-Azam University

Islamabad, Pakistan.

Submitted through:

Prof. Dr. Kashif Sabeeh

Chairman

Department of physics

Quaid-i-Azam University

Islamabad, Pakistan.

Dedicated to

My Supportive Family

Specially my Elder Brother (Abdullah shah)

And

Respected Teachers

Acknowledgment

*All praise to the Almighty **Allah** who enabled me to complete this research work successfully, without His will and consent we can't precede a single step. Millions of darood-o-salaam for The Holy Prophet **Muhammad** (peace be upon him), who is forever the foundation of knowledge and guidance for all humanity.*

*I feel honor to express my deepest gratitude to my supervisor **Prof. Dr. Raheel Ali**, for his scholarly guidance, generous encouragement, thought provoking discussions, pleasant attitude, ever helping and kind behavior throughout my research work.*

*This really gives me pleasure to thank my PhD senior **M. Bilal Shafique** for his keen interest and skillful help. My special thanks go to my senior **Muhammad Asif** for being friendly, helpful, and cooperative. I can never forget the continuously encouraging and friendly behavior of my lab mates Sadam Ali, Latif Ullah, Jamil Ur Rahman, Muhammad Noman and Mohsin Naeem, for their support.*

*I absolutely find no words to express my deepest feelings for my loving brothers **Dr. Abdullah Shah**, and younger one **Muhammad Atif** and my beloved sisters who put me on the right path.*

Last but not the least, I wish to express my deep gratitude towards my loving Parents. I believe, I did nothing more than their prayers did for me. May God bless them with health and happiness.

Akhtar Muhammad

ABSTRACT

An experimental study was conducted to observe the effects of inter-pulse delay on the generation of ions emitted during double-pulse laser ablation of an Aluminium target. A specific values of inter-pulse delay (550 ns, 570 ns, 600 ns, 650 ns, and 750 ns) were chosen from a delay generator using its second harmonic i.e., 532 nm to generate an Al plasma. The ion measurements are based on time of flight method, by using a time resolving plane ion detector, that was placed at a distance of 5 cm at the normal of the target's surface to measure the temporal variation of ions during the expansion of plasma in vacuum. The effect of inter-pulse delay on the average ion energy, total ion charge per pulse, kinetic energy distribution was investigated.

Table of Contents

List of Figures

CHAPTER 1

Introduction

1.1 Plasma

The plasma is a Greek word that interprets that something is primed or shaped. The matter of the universe is composed of almost 99% of the plasma state; that is when a gas is heated continuously, then the time will come that the electrostatic force which holds the electrons to the nucleus is affected by the thermal energy of its neighbor particles. In that situation, the atoms split up into positive ions and electrons which are named the fourth state of matter called "plasma".

A plasma is "a quasineutral gas of charged and neutral particles which exhibits collective behavior" [1]. To understand the definition of plasma we need to understand the terminology of quasineutral and collective behavior.

The term quasi means "as if" or "seemingly". "*Quasineutral*", describes the charge neutrality that is, neutral enough so that one can use the approximation $n_i \approx n_e \approx n$ where n represents the plasma density, but not sufficiently neutral that all the fascinating electromagnetic forces dissipate. By "Collective behavior" means motions that are influenced not only by localized circumstances but also by the state of the plasma in the far domain. Any ionized gas cannot be called a plasma, except that must fulfill the following three criteria;

i) $\lambda_D \ll L,$

ii) $N_D \gg> 1,$

iii) $\omega\tau > 1.$

Where λ_D is the length of Debye sphere, L is the dimension of the plasma, N_D is the number of particles in the Debye sphere, ω is the oscillation frequency of the plasma and τ is the meantime of collision between neutral atoms [1, 2].

Plasma is the plenteous form of matter in the universe, mostly present in the stars and intercluster medium. It is also present on the earth's surface naturally as well as artificially. There are various methods used to generate plasma.

i) Spark discharge method,

ii) Arc discharge method,

iii) Through the laser method.

We could use the laser-induced plasma in this project by targeting the material to become plasma by laser pulses. Laser pulses ablated material when struck on the surface. The ablated plume is expanding linearly as well as angularly. This plume is the plasma of the targeted material by laser pulses. The characteristics of the plasma depend upon the parameter of the laser pulses.

1.2 Laser Matter Interaction

When a target surface is focused by a laser pulse, a small section of material is separated from the surface due to melting, sublimation, or ionization, this is called laser ablation. PLA is a very useful technique for various purposes in different fields of science and technology; such as physics, plasma technology, engineering, molecular mass spectroscopy, chemistry, medicine, laser surgery, etc. PLA is a very simple experimental arrangement and can be easily adjusted according to the experimental context [3].

When an intense laser beam is directed toward a solid sample, the substance evaporates and highly ionized particles are ejected which causes a plume of the ablated material to form and grow angularly in the forward direction [4]. The laser pulses strike the target's surface and are absorbed by its atoms, heating the target's exposed volume. The solid's irradiated region experiences particle evaporation. The laser pulse continues to be absorbed, causing the creation of an ionized layer of vapors known as plasma that grows adiabatically in a vacuum [5]. Laser interaction with the target plasma system is shown

schematically in figure 1.1. It shows that during the time interval of incoming laser pulse, there occurs four different distinguishable regions: The unaffected solid target (A), the ablated material (B), the dense plasma that is absorbing laser energy (C), and the plasma transparent to the laser pulse (D).

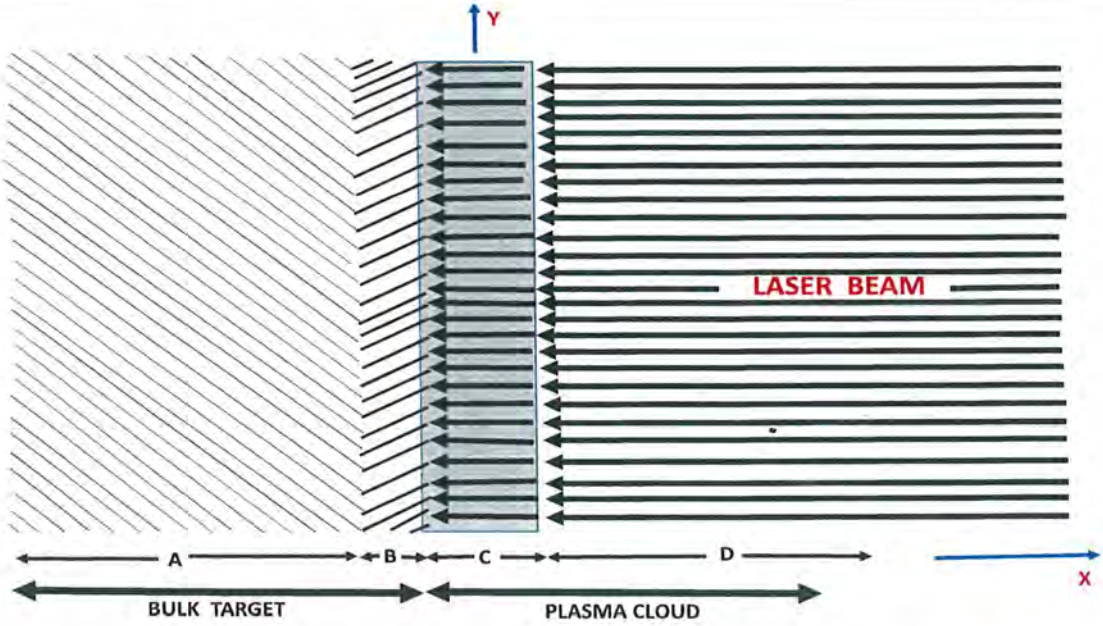

Figure 1.2 A schematic figure illustrating the existence of several zones during a laser pulse: the unaffected solid sample (A), the ablated target sample (B), the dense plasma absorbing the laser energy (C), and the plasma transparent to the laser pulse (D).

The ablation of a material by a laser depends on the laser's parameters (temporal width of the pulse, laser wavelength, laser energy), the material's properties (heating rate, melting, and evaporation, absorption and reflectivity, heat capacity, latent heat of fusion, density, thermal conductivity, sample phase), and the surrounding environment (gases species present in the chamber, vacuum pressure, etc.). The formation of plasma by picosecond and femtosecond laser is not enough good as compared to the nanosecond laser plasma. The energy and wavelength of the wave are inversely related, Because of the inverse relationship shorter wavelength lasers can ionize gas effectively by breaking the bond and ablating huge amounts of material. The rate of ablation is linearly influenced by laser fluence [6-9].

Numerous effects of the laser light are seen in the ablated material. It can be refracted, reflected, and absorbed by the plasma (plasma absorption coefficient). Thus, lasers heat the plasma, which is controlled by an absorption coefficient that depends on the plasma's temperature, density, and

wavelength. causing the isothermal expansion of the plasma. The oscillating electron interacts with the ions, which converts oscillating energy into thermal energy which drives the plasma's isothermal expansion. The sample phase, which is dependent on the media, also impacts laser-matter interaction. In solid samples, the conductive nature is responsible for plasma generation, while in semiconductor and dielectric materials, electron-hole pairs are produced and lead to vaporization. In gas and liquid samples, electrons are created to contribute to plasma.

1.2.1 Laser-mater Interactions Below the Plasma Ignition Threshold

The primary objective is to better understand the fundamental workings of PLA to have strict influence over the ablation operation, as the ablation process is highly dependent on the laser parameters, the optical and thermal features of the material, and the surrounding circumstances. The physics of PLA is highly complicated since it comprises interactions between laser and plasma, generation and expansion of plasma, and photon-matter interactions.

To acquire an exact understanding of the physical mechanisms all together, concerned with the phenomenon of laser ablation in the low fluence zone, Numerous theoretical and experimental research is currently ongoing. The solid sample heats up, melts, and evaporates at low fluence ranges. In this regime, a vapor plume that behaves as an optically thin medium is formed by the forefront of the laser pulse and the remainder of the laser pulse travels practically undetected through the plume.

There are now laser systems that can produce pulses with durations ranging from a few nanoseconds to around 100 fs. With these lasers, one can carry out an extensive examination of the laser-matter interaction at various laser pulse lengths while essentially maintaining the other laser properties [10-12]. Femtosecond and picosecond laser pulses are used for laser ablation, which can cause direct solid-to-vapor transformation. This makes it possible to treat metals and other materials with precision.

In the case of a nanosecond laser pulse, the material's surface absorbs the laser energy and heats to the melting point, where it subsequently reaches the vaporization temperature, which results in vaporization. In this instance, energy is consumed mostly by heat conduction into the solid sample and evaporation from the liquid metals. Laser radiation is absorbed by the free electrons found in metals. At femtosecond timescale the electron plasma is heated as a result of the e - e collisions and along with the e - e collision, e - ph collisions occur resulting in the energy transfer between the electrons and the lattice. Due to the substantial differences in the masses of phonons and electrons, the energy exchange resulting from e - ph collisions (of the order of picosecond timescale) lasts longer than the thermalization of electron plasma caused by e - e collision [13-17].

Some criteria are frequently satisfied depending on the laser system when the ablation of solid objects is concerned. When using femtosecond laser beams, where the period of the laser pulse is smaller than the hot electron relaxation time ($\tau_L \ll \tau_e$), the electron-lattice conjoining can be ignored. This is possible when $D_e\tau_L < \alpha^{-2}$ (i.e. The depth of thermal penetration is less than the depth of optical penetration.), where $D_e = k_e/C_e$ is the electron thermal diffusivity.

The irradiated material begins to evaporate significantly when $CT > \rho H_v$ (CT is the Compton temperature, which is a measure of the average energy of the photons in a beam of radiation, ρ is the mass density of the material, and H_v is the energy deposition rate). The condition for substantial evaporation is [12, 18].

$$F_a \geq F_{th} exp(\alpha z),$$

where F_a is the atomic flux, $F_{th} \sim \rho H_v/\alpha$ is the laser fluence threshold for femtosecond pulse-induced evaporation, α is the constant that depends on the properties of the material and the radiation, z is the depth of the material.

For picosecond lasers, the following circumstance is satisfied:

$$\tau_e \ll \tau_L \ll \tau_p,$$

where τ_e is the electron-phonon relaxation time τ_L is the laser-pulse duration, and τ_p is the plasma life time.

The electrons' cooling is caused by the lattice and the electrons exchange energy when the following condition is accomplished.

$$k_e T_e \alpha^2 \ll \Gamma_{e-p} T_e,$$

Where k_e is the electron thermal conductivity, T_e is the electron temperature, and Γ_{e-p} is the electron-phonon coupling constant, which is a measure of the strength of the interaction between the electrons and the lattice or phonons.

When dealing with nanosecond laser pulses, the circumstance that must be satisfied to ablate the solid targets are;

$$l_T \gg l_\alpha,$$

$$D_e t_e \alpha^2 \gg 1,$$

i.e. In comparison to optical penetration, thermal penetration is far deeper.

The solid's energy absorption per unit mass is calculated using [7]:

$$E = \frac{I_\alpha t}{\rho l_T}, \qquad (1.1)$$

here I_α is the intensity of the absorbed laser and l_T is the length of the heat diffusion. At a particular moment in time $t = t_{th}$, the deposited energy matches the latent heat of vaporization H_v, at which there is considerable evaporation occurs. From this we may deduce a relationship for the threshold laser fluence required for evaporation:

$$F_a \geq F_{th} \sim \rho H_v l_T. \tag{1.2}$$

The target surface experiences considerable evaporation when the surface layer of l_T thickness is heated to the melting temperature.

1.2.2 Laser-mater Interactions Above the Plasma Ignition Threshold

When plasma intensity exceeds the plasma ignition threshold intensity, the procedure for pulsed laser ablation has extremely complicated physics since it also comprises the generation and evaluation of plasma, and interactions between the laser and plasma in addition to direct laser-solid interactions. The primary mechanisms for laser light absorption in the ablation plumes generated on metallic targets are thought to be inverse Bremsstrahlung and photoionization processes [18, 19]. It has also to be considered the process of electrons transferring energy to ions and neutral entities, as well as electron influence processes such as excitation, ionization, and recombination, which occur in plasma dynamics [19]. Consider the adiabatic approximation while analyzing the laser-ablation mechanisms with extremely powerful nanosecond laser pulses or shorter pulse lengths. In this instance, the growth of the ablated mass occurs considerably more slowly than the laser absorption and the consequent processes of target thermalization, vaporization, and plasma production.

Due to the close proximity of the two stages (i.e., evaporation and plume expansion), a challenging interaction between the growing plume and the laser beam occurs. The laser pulse passes through the plume without experiencing any attenuation at low fluence levels because the vapor created by the forefront laser pulse, functions as a thin optical layer.

For high fluence value, plasma is generated above the target surface when metals are being vaporized by a nanosecond laser in a vacuum. The temperature of the vapor is adequate high that produce significant ionization of the entities that have been ablated, which compels the vapor to start absorbing the incident laser light, causing vapor breakdown and plasma production. Due to the large value of temperature and density of the laser-produced plasma, the target is effectively shielded while the laser pulse is being delivered [20-25]. The Plasma kinetic and laser-plasma interaction have a significant impact on the laser-ablation process.

1.3 Main Features of Laser-induced Plasma

The extremely complex mechanism of laser-matter interaction results in laser-induced plasma. When a laser beam is directed at a target, many simultaneous processes—laser energy absorption, vaporization, ejection, and fragmentation of atoms, ions, and molecular species—occur simultaneously, causing plasma. The plasma produced by a laser has some features:

i) To restrict the extent of the plasma and accomplish total absorption of laser energy, the particle density n essentially be sharp sufficient.

ii) Because of the energy demand, just a tiny amount of the thermalized material is required. Consequently, energy conservation;

$$E=3Nktv, \qquad (1.3)$$

where "E" denotes the absorbed energy of the laser and "V" denotes the volume of the substance heated to the temperature "T".

We assume that

$$n_i = n_e = n \qquad \text{(Quasineutrality)}$$

iii) The time length of the laser pulse will unavoidably constrain the lifespan of these values of n and T. The electron-ion equipartition period must be taken into account because we are working with freely growing plasma.

To approximate these, equipartition timings to expansion periods. We may infer that expansion will more effectively balance the lifespan of a hot spot in the plasma compared to the length of the laser pulse.

iv) Due to the plasma's high pressure, there will be a significant amount of expansion, which will result in temperature and density gradients inside the thermalized material. There are two key outcomes that this plasma blast-off will produce.

   a) Due to a greater number of particles absorbing laser energy, the plasma volume increases while temperature reduces as a result.

   b) A clear hydrodynamics behavior will manifest. Resulting in a restriction on the highest temperature that may be reached because of the conservation of internal energy into kinetic energy.

The aforementioned features of the plasma created by a laser are its most crucial ones.

1.4 Plasma Parameter

The key characteristics of plasma are its electron number density and temperature [26]. The use of plasma characteristics facilitates an understanding of the key processes, such as dissociation, ionization, and excitation. But the plasma must be taken into account in terms of local thermodynamic equilibrium (LTE) in order to determine these values.

1.4.1 Local Thermodynamic Equilibrium (LTE)

A system is said to be in thermodynamic equilibrium (TE) If it possesses the qualities listed below:

- All sorts of particle velocities maintain the Maxwellian distribution.
- Every energy level's population is distributed according to the Boltzmann law.
- The development of Ionization equilibrium is determined by the Saha equation.
- The explanation for the radiation's intensity is provided by Planck's equation.
- Each of the operations outlined above describes a physical phenomenon that occurs at a specific temperature, and each has its own temperature dependence.

Due to the fact that laser-induced plasma shouldn't be optically thick for a precise quantitative examination and can't completely absorb the radiations released, we investigate LTE rather than TE since the radiation equilibrium might not be reached as a result. Additionally, plasma temperature is only true precisely when plasma is in LTE [27].

Plasma temperature is account for an essential and fundamental parameter—expressed in electron volts (eV). The temperature of the plasma species (such as neutrals, electrons, and ions) does not always have to be the same. Also, the temperatures of the species parallel and perpendicular to the magnetic field may also differ if plasma is constrained in a magnetic field.

Application of the Boltzmann distribution law will reveal the relative population of excited states in an atom or ion [28].

$$n_k^S = n^S \frac{g_k}{\mathrm{P}(T)} \exp[-\frac{E_k}{K_B T}]. \qquad (1.4)$$

Where;

n_k^S =species S's excited level k population density,

n^S =The overall numerical density of the species S in the plasma,

g_k =The statistical value of the higher level of the transition,

P(T) =The partition function,

K_B = Boltzmann constant,

and

T=The excitation temperature (T_{exc}).

When used to explain the numerical densities of the same species at various phases of ionization, the Saha-Eggert equation may be written as follows [28]:

$$n_e \frac{{n_{Z+1}}^{\alpha}}{{n_Z}^{\alpha}} = \sqrt[3]{\left(\frac{2\pi m_e K_B T}{h^2}\right)} \frac{2P_{\alpha,z+1}}{P_{\alpha,z}} exp\left[-\frac{\chi_{\alpha,z}}{K_B T}\right]. \quad (1.5)$$

Where n_e is electron density, n_Z and n_{Z+1} is density of neutral atoms of element z and z+1 respectively, α is fine structure constant, m_e is mass of an electron, K_B is Boltzmann constant, T is the ionization temperature (T_{ion}), P is partition function, and χ is the ionization potential.

As LTE achieved, the velocity distribution function can be generated by using the Maxwell-Boltzmann distribution [29]:

$$f(v) = Av^2 \sqrt[3]{\left(\frac{m}{2\pi K_B T}\right)} exp\left(-\frac{mv^2}{2K_B T}\right). \quad (1.6)$$

In this expression A is normalization constant and T is the electron temperature (T_e).

Several mean velocities are defined here under the influence of the Maxwell-Boltzmann distribution function.

The formula for a particle's mean velocity is [30];

$$\bar{v} = \sqrt{\frac{8K_BT}{\pi m}}. \tag{1.7}$$

A single-dimensional average velocity is;

$$\bar{v}_x = \sqrt{\frac{2K_BT}{\pi m}}, \tag{1.8}$$

likewise, the rms velocity is;

$$v_{rms} = \sqrt{\frac{3K_BT}{\pi m}}. \tag{1.9}$$

In the reference of above given velocities, the total kinetic energy should be:

$$\bar{E} = \frac{1}{2}mv_{rms}^2 = \frac{1}{2}K_BT. \tag{1.10}$$

As it is abundantly evident that the temperature T affects both the average energy and the velocity of plasma species. As a result, the temperature T determines how the Maxwell distribution function for any particular plasma particles behaves.

The Maxwell distribution, Boltzmann distribution, and Saha-Eggert equation all apply to a single temperature known as the plasma temperature under local thermodynamic equilibrium;

$$T_e = T_{exc} = T_{ion}. \tag{1.11}$$

In order for LTE to exist, the interval between particle collisions in plasma must be shorter relative to the time span over which the plasma experiences any significant change. It is possible to assume that the LTE requirement will be met 1-2 milliseconds after plasma creation [31].

Most frequently, the LTE condition is examined using the Maxwell distribution criteria and McWhirter [32-34]. The Maxwell distribution criteria demand that $N_e > 10^{16}$ cm^{-3} and $kT < 5eV$ Furthermore, the McWhirter criteria stipulate that the pace of the radiative process must be 10 times lower than the rate of the collisional process.

Plasma has a stable macroscopic *charge neutrality*, which is another property. Internal space charge fields cause collective movements of particles when plasma deviates from the LTE condition in

order to maintain charge neutrality. These movements are parametrized by plasma frequency, that is electrons vibrates with the reference of massive ions since the ions can not follow the electron's motion to certain level due to the relatively massive nature to electrons. Usually, the electrons' oscillations is the plasma frequency, which is determined by [35]:

$$\omega_p = \sqrt{\left(\frac{n_e e^2}{m_e \varepsilon_o}\right)}. \tag{1.12}$$

To act like plasma, an ionized gas must have $\omega_p > \upsilon_c$. Where υ_c is the frequency of an electron colliding with a neutral atom.

Debye length is regarded as an essential and fundamental physical property used to characterize plasma. It provides details on the plasma distance at which the effect of electric field of one charged particle experiences by another. This separation is referring as "screening length or shielding length". When an external electric field is applied to plasma, that field exponentially weakens across the Debye shielding. Plasma temperature and electron density can determine Debye shielding, which is stated;

$$\lambda_D(m) = \sqrt{\left(\frac{\epsilon_o kT}{n_e e^2}\right)}. \tag{1.13}$$

The volume of charged particles inside the Debye sphere must be large enough for Debye shielding to be a statically sound idea i.e.

$$N_D = \left(\frac{4}{3}\pi\lambda_D^3\right) >> 1. \tag{1.14}$$

Within the vicinity of a distance equal to the Debye length, plasma is not neutral. It is the area where particles organize themselves in such manner to either nullify the impact of an externally applied field or create a transition layer between the plasma's edge and the plasma itself. Debye length can alternatively be thought of as the distance at which local variations in space charge are balanced out. Charge neutrality is preserved when the dimensions of the plasma exceed λ_D, If the plasma's dimensions are lower than λ_D, spatial oscillations take place as a result of which charge neutrality is no longer remains retained.

1.5 Effect of Laser Parameters on Plasma Temperature

The experimental settings have an impact on both analytical execution and plasma operation. Numerous variables, including laser parameters (such as laser wavelength, pulse frequency, laser energy, and dual laser mode), and ambient environment, affect the temperature of plasma induced [36-38]. The result shows that generally LIP temperature typically rises when laser parameters (such as pulse width, energy), background gas pressure, and sample hardness increase. The conclusions indicate that, in general, LIP temperature rises when laser parameters (such as pulse width, energy, and laser wavelength), background gas pressure, and sample hardness increase. But with growing separation from the sample surface, it diminishes.

1.5.1 Laser Wavelength

Utilizing lasers with the same pulse widths (of 5 ns) and irradiances (of $5 \times 10^{10}\ Wcm^{-2}$) at 1064 nm, 532 nm, and 355 nm on zinc and cadmium targets in the presence of He, Ne, and Ar, it was discovered that temperature rises with increasing wavelength. It has been proposed that the absorption of the primary photon energy derives from inverse Bremsstrahlung (IB) mechanism, in which electrons acquire kinetic energy through collisions with ions and neutrals, which excite the plume. The IB mechanism is particularly crucial when using longer wavelength lasers since the 1064 nm laser has significant IB absorption and generates plasma at a higher temperature than the 532 nm and 355 nm lasers [39-42].

When using laser beams with wavelengths of 1064 nm, 532 nm, and 355 nm with fluences that range from $3 \times 10^{10}\ Wcm^{-2}$ to $9.87 \times 10^{10}\ Wcm^{-2}$, it was found that the temperature of lead plasma rose as the laser wavelength goes down [43]. It was also investigated that the Sn sample using a 1064 nm laser, which produces a lower temperature than 532 tum and 355 cm laser beams because less mass is ablated due to a shallower penetration depth into the Sn sample [44].

1.5.2 Laser Pulse Width

Generally, the temperature of laser induced plasma elevates with the incrementation of laser pulse width. Two lasers (800 nm, 100 fs; 1064 nm, 8 ns) with the same irradiance of $20\ Jcm^{-2}$ were used to investigated an aluminum sample in the atmosphere in a spatially integrated way across a temporal frame of 200 ns—25. It was noticed that the temperature of the produced plasma with the ns laser was comparatively higher than fs laser because the duration of the ns laser is adequate for interacting with the

plasma and causing the plasma to heat up [45]. After a predetermined period of time (for example, 1 μs), radiation cooling takes precedence over expansion cooling in plasma, hence various pulse widths were employed and found roughly the same temperatures [46, 47].

1.5.3 Laser Energy

Most often, LIP temperature rises as laser energy rises. Laser with a range of energies (1064 nm, 7 ns, $625\,Jcm^{-2}$–$11875\,Jcm^{-2}$) were used to study the fluctuation in plasma temperature. The observations manifest that the plasma expanded more quickly during the time frame of 0.5-8 μs which caused the temperature to drop quickly. When the laser energy is intensified, the temperature rises; however, when the laser irradiance reaches a particular limit, the temperature remains constant and becomes saturated [48].

The investigation of YBCO samples in vacuum with a 1064 nm, 9 ns laser, while adjusting the laser energy ($15\,GWcm^{-2}$–$70\,GWcm^{-2}$), results that raising the laser energy causes temperature to rise, and the saturation hit at $54\,GWcm^{-2}$ because of the plasma shielding (i.e., reflection and absorption) [39, 40, 49]. The laser light is reflected from the plasma under the condition that is $v_l < v_p$. Where v_l denotes the laser frequency and v_p denotes the plasma frequency, which may be calculated as:

$$v_p = 8.9 \times 10^3 N_e^{1/2}. \tag{1.15}$$

Because of the IB, the plasma absorbed more energy at high laser energy in comparison to the target itself, resulting in less material vaporization than at lower energy. On the other hand, the Cu plasma using a 532 nm, 15 us laser with variable laser intensity ($45\,Jcm^{-2}$–$120\,Jcm^{-2}$), Results that raising the laser intensity caused temperature to rise, and that after reaching a saturation zone, temperature began to fall at $45\,Jcm^{-2}$ as energy was absorbed and reflected by the air plasma formed above the target surface [50].

1.5.4 Dual-pulse Laser Mode

Generally, research publications demonstrated that the temperature of plasma created by a dual pulse (DP) laser configuration is greater than that of a single-pulse laser configuration (SP). Laser with a range of energies (532 nm, 8 ns, ($1.19 \times 10^{10} - 2.04\,Wcm^{-2}$) were used to investigate the comparison of DP and SP plasma temperatures in Sn plasma in the atmosphere. The observations manifest that the plasma temperature increases while utilizing DP mode during the time frame of 0-6000 ns. When using

the second laser in the DP mode, it may readily enter the plasma's core, which has a lower shielding effect than when using the SP mode [51-54].

The Cu plasma generated with 248 nm, 450 fs laser by adjusting laser intensity ($0.57\,Jcm^{-2}$–$5.66\,Jcm^{-2}$) was investigated with the time frame of Δt: 200 ps between two lasers in the exposed environment for both SP and DP modes. As a result, the plasma's temperature caused by the SP mode dissipated more quickly than the DP mode [52]. The temperature of steel plasma, under the condition of laser (1064 nm, 80 mJ, 15 ns for SP, and 25 ns for DP) reveals that, compared to SP mode, temperature saturation in DP mode occurred at greater energies [53].

The temperature is also governed by the time period between the two lasers (Δt) and the distance between the lens' focus point and the target surface (d). The temperature didn't alter with Δt when $d < 0.7$ mm, however it did reach a low value at roughly 1000–3000 ns Whenever $d > 0.7$ mm. This occurred in the pre-ablation DP mode with varied laser intensities while maintaining the same pulse width and wavelength [54]. The investigation of aluminum plasma in spatially integrated methodology with varying Δt from 0 μs to 50 μs reveals that the plasma's temperature will be at its highest for Δt between 1 to 7 μs [55].

1.6 Plasma Plume Expansion

The term "ablation plume" refers to a collection of particles that are expelled from a solid as a result of laser matter interactions. These particles may include ions, neutral atoms, and even droplets or clusters of molten material.

The mechanical, electrical, and chemical characteristics of the plasma plume's constituents vary. The speed and perpendicular orientation of all ablated species' ejection, determines the plume's propagation.

There are several sorts of interactions and forces taking part in such procedures that influence plume dynamics. A high density of particles will be expelled at short time spans and travel linearly, interacting and influencing each other's velocity. These interactions lead to the plume growth by expanding plume dimensions in all directions and influencing plume size and form. The movement of plume particles in a direction normal to the original velocity as a result of these interactions produces the most glaring effect, which is an explosion of the plume superimposed over its linear initial motion.

Mechanical interactions are the primarily and frequent interactions throughout the transmission and expansion of plasma, because of the plasma plume's high proportion of neutral particles (i.e., more than 95%). These interactions happen as a result of particle collisions inside the plume or with surrounding gas particles. As collisions are a statistical approach, they are influenced by the density, size, and speed of the particles. So, statistically, just after laser interactions with matter, Because of the high plume density collisions between plume particles would be the most prevalent interaction. The moment the plume begins to grow, it begins interacting with the surrounding gas particles. Later, after the plume has extended to a few centimeters from the sample surface, collisions between the plume's particles will become minimal, while the contact with surrounding gas particles will take precedence.

Electrical interactions are another sort of interaction that is seen as being less important in plume dynamics but is extremely important in the early phases of plume expansion. The charge density reaches its highest right after particles are ejected from the solid and tends to aid in the plume's growth. The charge density peaks right as particles are ejected from the material and tends to aid in the plume's growth. Electrons travelling more quickly to the limits of the plume while ions move more slowly behind them due to mass differences. They interacting with one another and causing expansion at these early phases. In literature, when the plume front is polarized with ions within and electrons outside, is referred to as a plasma double layer. As time goes on, the recombination procedures take place, which reduces the overall charge. Additionally, as the plume expands, the electrical forces of contact between charged particles begin to weaken with lengthened distances between plume particles and eventually become insignificant for plume propagation.

After plasma production, an increase in laser irradiation caused the plasma's temperature and density to rise. When a material is heated by a laser beam, some of the energy is transformed into the particles' thermal and some into ionization energy, which causes a rise in thermal pressure and plasma temperature. The rise in thermal pressure causes the plasma to expand. The expansion of plasma reduces its density. Thus, some of the laser energy might be transformed into plasma kinetic energy during the expansion phase.

1.7 Mechanism of Laser-light Absorption

The interaction of the ablated sample with the residual laser pulse causes plasma heating, which is regulated by two different absorption processes. The first is *inverse bremsstrahlung* which dominates

for $I\lambda^2 > 10^{15} W\mu m^2/cm^2$, second is the *photoionization* which dominates for $I\lambda^2 < 10^{15} W\mu m^2/cm^2$ [30]. Both methods transform laser energy into plasma thermal energy, resulting in a large plasma ionization. So, before discussing these methods, it is important to formulate the classic Saha equation for single-charged ion species density (*ni*) in a gas at LTE circumstances [56].

$$n_i = \sqrt{2.4 \times 10^{15} T^{3/2} n_n exp(-I_1/k_B T)}, \tag{1.16}$$

where T is temperature in K, n_n is neutral's density in cm^{-3} and I_1 is the gas atoms' initial ionization potential in eV.

1.7.1 Inverse Bremsstrahlung

When free electrons collide with ionized and neutral constituents, they undergo a collisional process known as inverse bremsstrahlung in which laser light is absorbed. In a laser beam's electromagnetic field, the free electrons oscillate at laser frequency ω with a velocity of v_e [30].

$$v_e = v_{osc} sin(\omega t), \tag{1.17}$$

where v_{osc} stands for oscillations' amplitude.

The electrons' increased kinetic energy by colliding with neutrals in the ground state and excited state, enhance the degree of ionization. When the ion density is large enough, the IB caused by electron-ion collisions is almost twice as great in magnitude as that caused by electron-neutral collisions. Simply said, neutral atoms have a lower probability of absorbing photons than ions do.

The IB absorption coefficient α_{IB} with frequency ν of radiation is provided by [56]:

$$\alpha_{IB} = 3.7 \times 10^8 \frac{Z^3 n_i^2}{T_e^{1/2}} [1 - exp(-h\nu/k_B T_e)]. \tag{1.18}$$

Where;

T_e = electron temperature in eV,

n_i = is ion density,

and

$Z =$ is the ionic charge state.

The preceding equation illustrates that raising the frequency improves the efficiency of the IB process. As plasma absorbs through the IB process, its temperature rises and it gets more ionized, resulting in more effective absorption.

The intensity of plasma plume ionization and the effectiveness of the ablation procedure are both factors that affect α_{IB}. So, the IB absorption coefficient α_{IB} may be calculated using the optical, thermal, and ablated material parameters, including ionization potential. This process may involve photoionized electrons as well as electrons ionized by a collision of electrons. In the initial stages of laser-solid interactions, immediately evaporating electrons from the sample may contribute significantly to IB absorption.

1.7.2 Photoionization

For laser ablation techniques using visible and ultraviolet light, the Photoionization of excited atoms is more efficient, while inverse bremsstrahlung is less effective. For this procedure, the absorption coefficient is approximately given by [7, 57].

$$\alpha_{PI}(cm^{-1}) = \sigma_{PI} N_n \approx \sum_n 2.9 \times 10^{-17} \frac{\varepsilon_n^{5/2}}{(h\nu)^3} N_n. \qquad (1.19)$$

Where,

σ_{PI} is a photoionization cross-section,

N_n is the number density of excited state n,

ε_n is ionization energy in eV,

and

$h\nu$ is photon energy in eV.

The summation will only be applied to those energy levels that meet the following criteria:

$$h\nu > \varepsilon_n.$$

In metals, photon energy is almost equivalent to the energy required for the ionization of excited atoms. Additionally, a large number of excited atoms result from Plasmas created by nanosecond lasers that have tremendous temperatures and densities, these atoms may further be photoionized by visible and UV light. Furthermore, it has been found that the time constants for electron impact ionization and excitation are substantially shorter than the laser pulse duration, which effectively improves the ionized and excited constituents [58, 59]. This rise in electron and ion concentrations raises the probability that IB will absorb photons as a result of electron-ion interactions.

The electron generation by PI (Photoionization) and EI (Electron Ionization) can be balanced by recombination activities, which reduces ion density in plasma. The electrons generated by PI and EI will help improve IB absorption if the recombination period is equal to or larger than the duration of the pulse.

1.8 Ion Kinetic Energy Distributions

It's possible to determine the kinetic energy of ions using the velocity distribution of ions and the other way around. Both velocity distribution (VDs) and kinetic energy distributions (KEDs) are commonly used in plasma characterization, as they are both important. When a sample is struck by a strong laser beam, plasma form instantly and begins to expand adiabatically in the vacuum, with ions possessing kinetic energy ranging from a few electron volts to several kilo-electron volts. The emission of ions from a laser-induced plasma (LIP) is not uniform in all directions. The energy of the ionized atom is determined by the plasma's temperature, and they move due to coulomb acceleration caused by the plasma's generated electric field. The ion kinetic energy is influenced by both the charge state and laser fluency [60]. The final ion velocity is affected by three factors, including thermal velocity, plasma expansion velocity, and velocity due to coulomb acceleration.

The thermal velocity is determined by

$$v_T = \sqrt{\frac{8kT_s}{\pi m}}, \tag{1.20}$$

where, T_s is the surface temperature, which is defined as;

$$T_s = \frac{F(1-R)\alpha}{\rho C_p}, \tag{1.21}$$

and F, R, ρ, α, C_p stand for laser fluency, solid reflectivity, density, absorption coefficient, and heat capacity, respectively [61].

The velocity of plasma expansion is defined as

$$v_k = \sqrt{\frac{\gamma kT}{m}}, \tag{1.22}$$

where, γ is the coefficient of an adiabatic expansion.

The velocity due to coulomb acceleration is given by

$$v_c = \sqrt{\frac{2ezV_a}{m}}, \tag{1.23}$$

where, V_a is the voltage for acceleration.

The summing of v_k and v_c results in a shift of the Boltzmann distributions toward higher energy [62]. The ion velocity distributions beyond the ablation threshold fit to a shifted Maxwell-Boltzmann Coulomb distribution, since thermalized ablated constituents follow the Maxwell-Boltzmann distribution, as predicted by Torrisi [63].

$$F(v_x) = A\left(\frac{m}{2\pi kT}\right)^{\frac{3}{2}}(v_x)^3 \exp\left[-\left(\frac{m}{2kT}\right)(v_x - v_k - v_c)^2\right]. \tag{1.24}$$

Where, v_x is the velocity of atoms along the target normal, v_k is the velocity of plasma expansion, and v_c is the velocity resulting from the coulomb potential.

1.8.1 Methods of Investigating Ion KEDs

The KEDs of ions have been studied using a variety of approaches. Two of them are commonly employed that is the time-of-flight (TOF) profile method and the energy analyzer, which is used to discriminate energy. Here we employed the TOF profile method to evaluate the KEDs of ion.

Fast diagnosis and the ability to extract the most distribution from a laser pulse are two benefits of TOF techniques that make them an efficient tool for plasma diagnostics. The reason behind this is that the time it takes for ions to arrive at the ion detector is far longer than the time it takes for them to produce ions. And also the ion KEDs of ions may be simply obtained from spectra of the TOF method. The TOF techniques are typically classified into two components.

In the first section, there are a number of ion-collecting techniques that may be used with a Langmuir probe or a set of faraday cups to look at the angular or spatial development of plasma. The second section is optical emission spectroscopy (OES), which assist in characterizing the excited atoms. Furthermore, ion detectors paired with a retarding potential enable ion-collecting approaches to overcome mass unresolved obstructions, which is beneficial for kinetic energy diagnostics [64, 65].

CHAPTER 2

Experimental Setup

The experimental conclusions that are presented in this research project were obtained from the experiments conducted at Quaid-e-Azam University's Atomic and Laser Spectroscopy Laboratory in Islamabad. The entire experimental setup is illustrated in figure 2.1. The sample was ablated and plasma was produced utilizing two Quantel Brilliant Nd: YAG laser systems at wavelength of 532 nm corresponding to the second harmonic of the laser. An ion detector was utilized to collect plasma placed at 5 cm away from the sample surface. The target used in this experiment was an aluminium (Al) with a surface area of 2.54 cm^2 and a thickness of 2 mm. To oppose the electrons and obtain a perfect ion signal, the ion detector was given a negative voltage i.e., $-30\ V$, using dry batteries. To ensure that every laser fire strike a smooth surface, the sample was positioned on a target stand that was manually rotated from outside the chamber. The entire apparatus was placed inside a 22 cm diameter, finely designed cylindrical stainless steel container with many apertures of various flange diameters. With the support of an oil diffusion pump, the system's pressure was kept at around $10^{-5}\ mbar$, and a Penning gauge was used for measuring the pressure. The two beams were aligned on to the sample employing 532 nm mirrors. The beams were focused on the sample surface using a 50 cm convex lens. Furthermore, an electric feedthrough was used to transmit the ion signal from the probe to an RC circuit. In addition, the signal that was captured across the RC circuit's resistance was displayed on an oscilloscope (TDS 2024), and stored on a PC for analysis. The schematic diagram of the entire experimental apparatus is illustrated in figure 2.2.

2.1 Laser Systems

LASER is an abbreviation of Light Amplification by the Stimulated Emission of Radiation. It is a light-amplifying apparatus that emits a narrow range of wavelengths beam that is extremely intense and directional.

Following are some distinguishing qualities of lasers that set them apart from regular light:

- It is nearly monochromatic, i.e., comprises a very limited spectrum of wavelengths.
- It is highly coherent, i.e., The motion of photons is synchronized (in phase).
- It is highly directional i.e., Traversed in a single direction within a small cone of divergence.

Figure 2.1: *Experimental setup for studying ion emission of Al.*

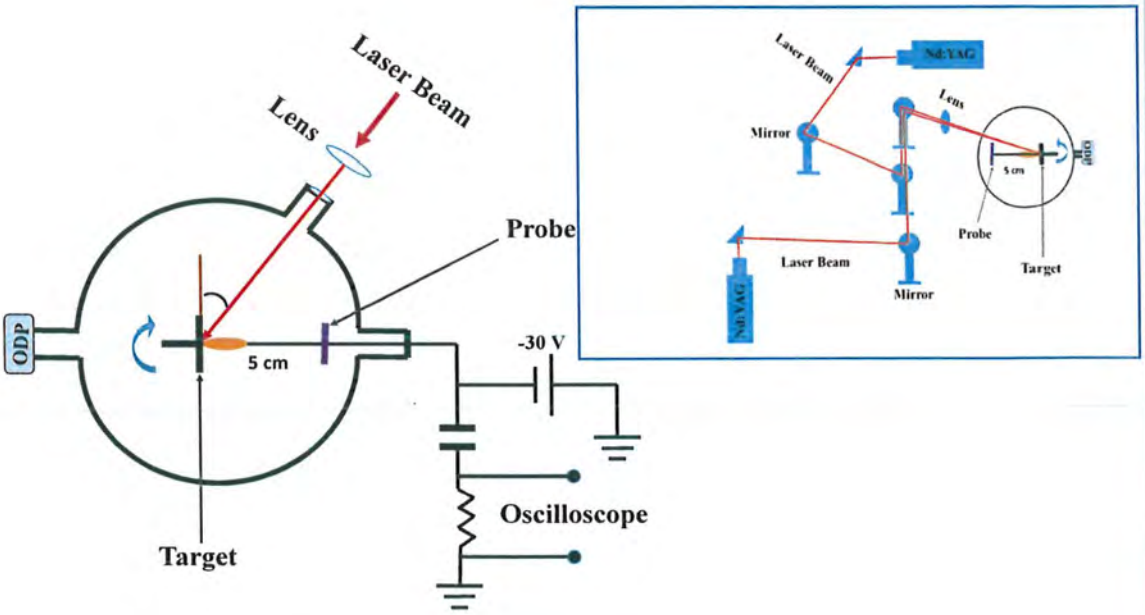

Figure 2.2: *Schematic diagram of experimental setup.*

ODP: Oil Diffusion Pump

There are three parts that need to be carefully examined while building a laser as shown in figure 2.3.

1) first and foremost, an active media can be a gas, a liquid, or a crystal.

2) Second, an excitation process, which may be optical, electrical, or thermal, is necessary since the primary goal is to produce population inversion in the active medium.
3) The third element is the laser resonators, which are typically constructed by aligning mirrors (either planar or curved) with the axis of laser light transmission in order to magnify the photons that are stimulated to emit. One of the mirrors has a coating that ensures 100% reflection of the laser wavelength, while the other has a coating that ensures around 90% reflection. This mirror also provides out beam as a laser light.

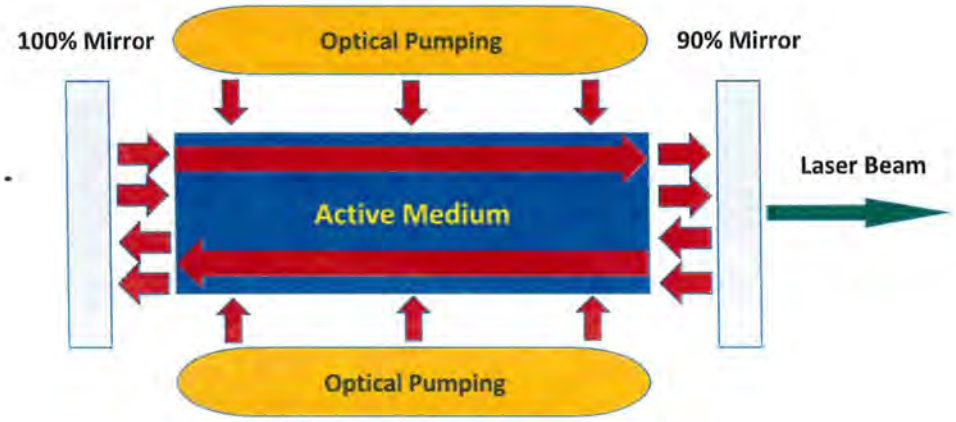

Figure 2.3: Components and Working of Laser.

A laser reaction requires three different sorts of operations that involve the interaction of light beams with atoms that have electrons in varying energy levels (i.e., spontaneous absorption, spontaneous emission, and stimulated emission). Any substance exposed to light undergoes several excitations and de-excitation reactions. Absorption process happens at the lower level, whereas spontaneous and stimulated emission happens at the higher level.

The population of distinct levels is determined by the Boltzmann relation at thermal equilibrium, which indicates that the population of the upper level is smaller than that of the lower level. In this case, spontaneous emission takes precedence over stimulated emission.

$$N_i = Aexp(-\frac{E_i}{kT}),$$

where,

N_i =Population Number,

k =Boltzmann constant,

E_i =Energy of level i (By assuming that $E_{i-1} < E_i$ i.e., $E_2 > E_1$),

and

A =Proportionality constant.

So the difference in population number (N_1, N_2) between the two energy levels E_2 and E_1 is;

$$N_1 - N_2 = N_1[1 - \exp(-\frac{h\nu}{kT})], \qquad (2.1)$$

where,

$\nu = \nu_2 - \nu_1$ is the frequency of the energy difference between the two levels E_2 and E_1.

Stimulated emission of radiation is an important process in lasers. The idea of stimulated emission was initially proposed by Albert Einstein. It was previously thought that a photon could only interact with an atom in two ways: either by absorbing the photon and moving up an energy level or by emitting the photon and moving down an energy level. Another hypothesis put out by Einstein was that an atom in a higher energy level may be stimulated to drop down to the lower energy level by the emission of a second photon with the same energy and phase. This would need a photon with energy equal to the difference between the two energy levels.

The population of the higher level and the energy density of the incoming photon both affect the rate of stimulated emission.

$$W_{21} = B_{21}N_2\rho(\nu_{12}), \qquad (2.3)$$

where the proportionality constant B_{21} is known as the *Einstein B coefficient* for that particular transition, N_2 is the population of higher energy levels and $\rho(\nu_{12})$ is the energy density of incoming photons.

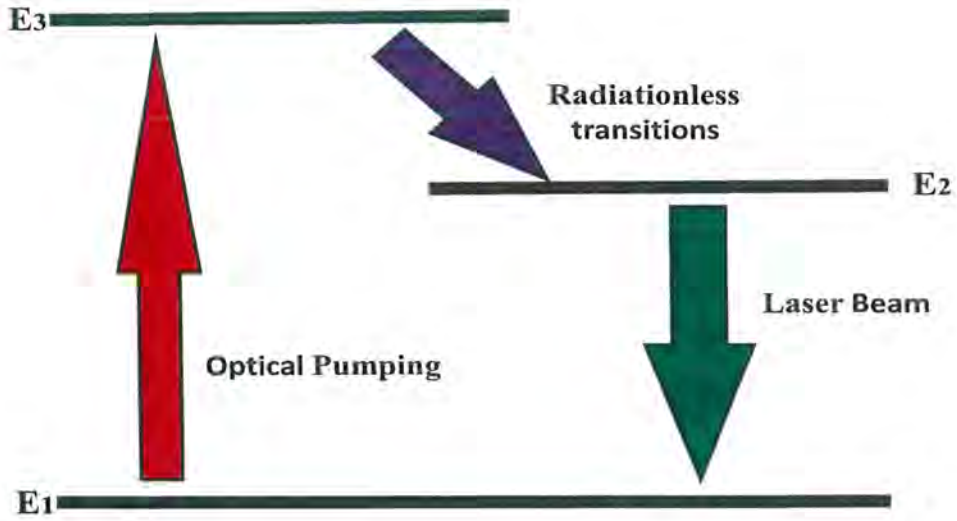

Figure 2.4: Three level system showing different processes to achieve laser activity.

To perform the laser action, the condition of population inversion must be satisfied that is The population number of the higher level must be greater than the population number of the lower level in order for stimulated emission overcomes absorption. Furthermore, electromagnetic radiation's energy density should be as high as possible.

In order to accomplish population inversion and produce a laser beam, a three-level system is illustrated in Figure 2.4. Atoms were continuously pumped by a pumping process from their ground state (E_1) to their excited state (E_3) to start the laser activity. The excited state (E_3) is set with a lifetime that is exceedingly short—roughly 10^{-9} sec, for that reason Atoms rapidly decay to a metastable state (E_2) with a lifespan of the order of a few milliseconds. Atoms continued to accumulate at the metastable level, allowing for a population inversion between the ground state and the metastable state.

When an atom is de-excited to ground level while emitting photons, the other atoms in a metastable condition are further stimulated by that photon's emission to do the same. In order to stimulate additional emission, two reflecting mirrors were positioned at either end of the active medium, which reflected these photons back into the cavity. This cycle is repeated until a stable equilibrium is reached where the overall gain equals the total losses in the cavity.

2.1.1 Neodymium YAG Laser

General Description:

We employed two similar Nd: YAG laser system in this experiment in order to ablate the palladium sample, both these laser systems were from Quintel. The laser head of one of the system is shown in figure 2.5. Nd: YAG (Neodymium doped Yttrium Aluminum Garnet) laser is a solid-state laser and it is one of the most frequently used laser media for a variety of scientific purposes. It is an illustration of a four-level laser system and can be used in both continuous and pulsed modes. In this instance, Neodymium (Nd) is used as the active medium, while YAG ($Y_3Al_5O_{15}$) crystal acts as the host. Nd^{+3} ions are doped into a YAG crystal at a doping concentration of roughly 1% by taking the place of certain Y^{+3} ions in the YAG. A xenon or krypton flash lamp is then used to pump it, producing a laser beam with a wavelength of 1064 nm. By employing the second and third harmonics, one may also create laser beams with wavelengths of 532 nm.and 355 nm., correspondingly.

Excitation Mechanism:

The four Nd^{+3} ion levels are graphically illustrated in figure 2.6. The first level $^4I_{9/2}$ is the ground level, the second level is $^4I_{11/2}$, and the third level is $^4F_{3/2}$, while the fourth level of the system is $^4F_{5/2}$. When the flash lamp is activated, it releases powerful radiation. These radiations were previously absorbed by the ground state ($^4I_{9/2}$) atoms and are transmitted by optical pumping to the $^4F_{5/2}$ state.

The atoms subsequently undergo a radiationless decay to the lower metastable state $^4F_{3/2}$ via lattice phonons. This level has a lifespan of 230 μsec, so atoms will stay there for a longer period of time, making it the upper level for the laser action. Thus, population inversion is achieved and atoms then undergo a lasing transition to the $^4I_{11/2}$ and $^4I_{9/2}$ at wavelengths of 1064 nm and 946 nm, correspondingly. This system has excellent quantum efficiency because of the rapid radiationless decay from the $^4F_{5/2}$ level to the $^4F_{3/2}$ level, which happens in around 10^{-7} seconds. However, the most likely transition for lasing activity is to the $^4I_{11/2}$ level, which has the greatest stimulated emission value and the lowest lasing threshold. Following this transition, Nd atoms rapidly relax from this level to the ground level. Consequently, each time a flash lamp is ignited, photons with a wavelength of 1064 nm are created.

Figure 2.5: Nd:YAG Laser System

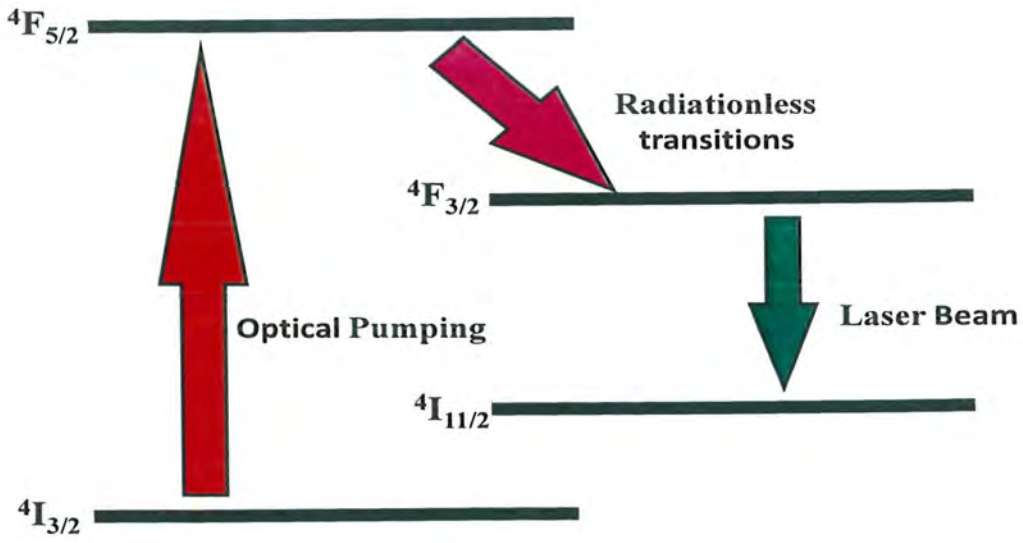

Figure 2.6: Energy level diagram of Nd: YAG laser.

The Nd: YAG laser's peak power is low and its pulse duration is lengthy, thus a Q-switching approach is employed to decrease the pulse duration and boost the output laser's peak power in order to

get a shorter pulse and higher peak power. The Q-switching process in Nd: YAG lasers is carried out by positioning an electro-optical component inside the laser's cavity.

Q-switching:

A procedure that involves isolating the cavity from the laser medium by enclosing the cavity in a closed shutter, which is essentially the Q-switch is there inside the cavity. The shutter opens as soon as laser pumping is finished, reestablishing the cavity's Q. The following are some essential conditions for efficient Q-switching:

1) In order to create a sufficiently substantial population inversion, the pumping rate must be higher than the upper lasing level's spontaneous decay rate.
2) The initial cavity losses must be considerable during the pumping duration to prevent beam development and oscillations.
3) In order for the beam to grow and extract excess energy that had previously accumulated in the higher laser level of medium, the cavity losses must be instantly decreased by abruptly adding high Q cavities.

Electro-optical Q-switch:

Some materials, known as optically active materials, have the capacity to rotate the polarization plane of light traveling through them. The electro-optic effect, which is a similar phenomenon, is observed in certain materials when an electric field is applied to them. The electro-optic materials can function like a fast Q-switch. To polarize the output laser, a polarizer must be placed in the cavity beside the crystal as illustrated in Figure 2.7.

The crystal serves as a quarter waveplate and rotates the plane of polarization at a 45° angle as a voltage is applied. This results in the conversion of linearly polarized light to circularly polarized light. The mirror reflects the beam, which then bounces back through the cavity in the opposite direction. Its plane rotates an extra 45 degrees as it passes through an electro-optic cell, thus the plane-polarized light is polarized at a 90 degrees angle to the initial direction.

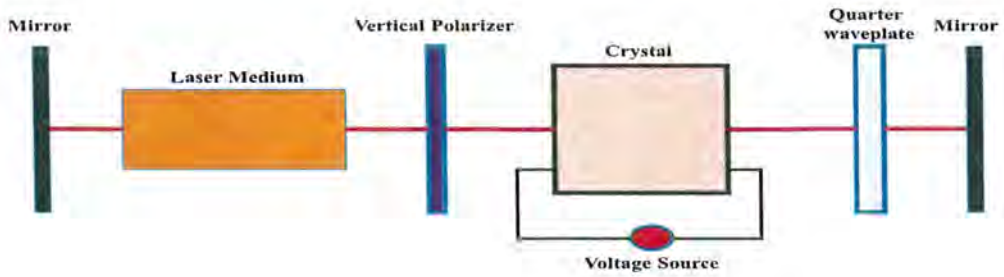

Figure 2.7: Q-switching Diagram

This light cannot get through the polarizer, therefore the cavity is turned off. The plane of polarization does not rotate when the voltage is zero, and Q-switching takes place. The voltage shift that is synchronized with the pumping mechanism may take less than $10\,ns$ to produce, leading to extraordinarily efficient Q-switching.

2.2 Vacuum System

A stainless steel vacuum chamber that was evacuated with the help of an oil diffusion pump makes up the vacuum system. The following is a description of both of these elements:

2.2.1 Vacuum Chamber

The vacuum chamber that was utilized in this experiment was expertly crafted from stainless steel and had a cylindrical form, as illustrated in figure 2.8. The chamber has a 22 cm diameter having multiple apertures, including four smaller apertures with a diameter of approximately 2 cm and six larger openings with a diameter of around 4 to 5 cm. Every opening is locked with an O ring and serves a distinct purpose depending on the demands of the experiment. Pressure blanks are used to conceal the openings that are not in demand. It contains two quartz windows, one measuring roughly 7 cm in diameter at the top of the cylinder and the other measuring about 4 cm in diameter on the side. One of its apertures is equipped with vacuum feedthrough. It is typically, a conductor deployed to convey an electrical impulse through

an enclosure. The feedthrough utilized in the research is an electronic feedthrough, which consists of a copper conductor that permits a voltage impulse of 5 kV and 10 A to transit through it.

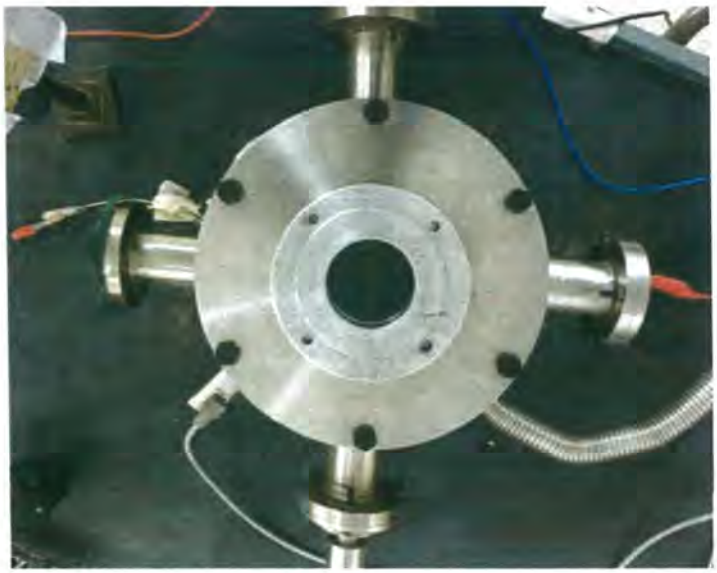

Figure 2.8: Vacuum Chamber (Top view).

2.2.2 Oil Diffusion Pump

An Oil Diffusion Pump is an apparatus, in which massive fluid molecules move at incredible speeds in the form of vapors, interact with the air molecules to be evacuated, and then influence the flow of molecules in a certain trajectory in the direction of the pump's exhaust. The name "diffusion pump" or "vapor jet pump" was coined due to the pump's pumping process, which is relied on the diffusion of gas molecules in a vapor jet. A clean atmosphere devoid of any potential oil vapor contamination was necessary for the majority of applications. ODP is used to reach such conditions and high vacuums, however additional safety measures are then required.

2.2.2.1 Working Principle

The ODP's operating principle may be described with the help of Figure 2.9. A boiler is used to heat oil to a vapor pressure of 1-2 $mbar$ from its initial high molecular weight, normally 400–500 amu,

and low vapor pressure state. These boiled vapors pass via funnels and are released through three or even more jets into an area of lower pressure, which was regulated at around 10 $mbar$ or less with the power of a rotary pump attached to the exit. The vapor stream is smooth while moving via funnels but becomes turbulent and molecular when exiting through funnels. The jet moves in the manner of a spreading skirt that expands downward and outward to the interior wall of the pump as a result of the expansion via the nozzles. This wall is cooled by water flowing through capillary pipes made of stainless steel that are looped around the wall of the pump. In this location, the vapor condenses and transforms back into liquid, which then flows through the wall and back into the boiler where it is heated and vaporized once more. Consequently, a continual cycle is initiated. If the gas pressure is low enough at the intake that it has molecular behavior, the fast-moving moving oil molecules probably will interact with the air molecules that drift into the jet. which will give them an extra downward velocity and lead them to travel through it toward the bottom of the pump. The pumped air keeps flowing at a higher pressure to the bottom section of the pump, passing through the exit where it is pressed and withdrawn with the aid of a mechanical backup pump, and finally discharged.

The gas molecules should not be in a fluidic state because if they are, the jet will be broken up and the pumping activity would be destroyed. In order to attain molecular circumstances, the main pump was utilized to minimize the pressure at its intake to roughly 0.1 $mbar$. After that, ODP dramatically decreases the pressure in the chamber attached to its intake.

In addition, the jet serves as a seal between the high-backing-pressure pump input and exit, which stops the backflow from exit to intake. The backflow from exit to intake sealing occurs only if the backup pump successfully kept the output pressure below a critical level. This critical value, also known as the critical backing pressure, corresponds to around tenths of the boiler's vapor pressure, which is what creates the jet. In any other scenario, the overpowering jet action coming from the outlet side stops the pumping activity.

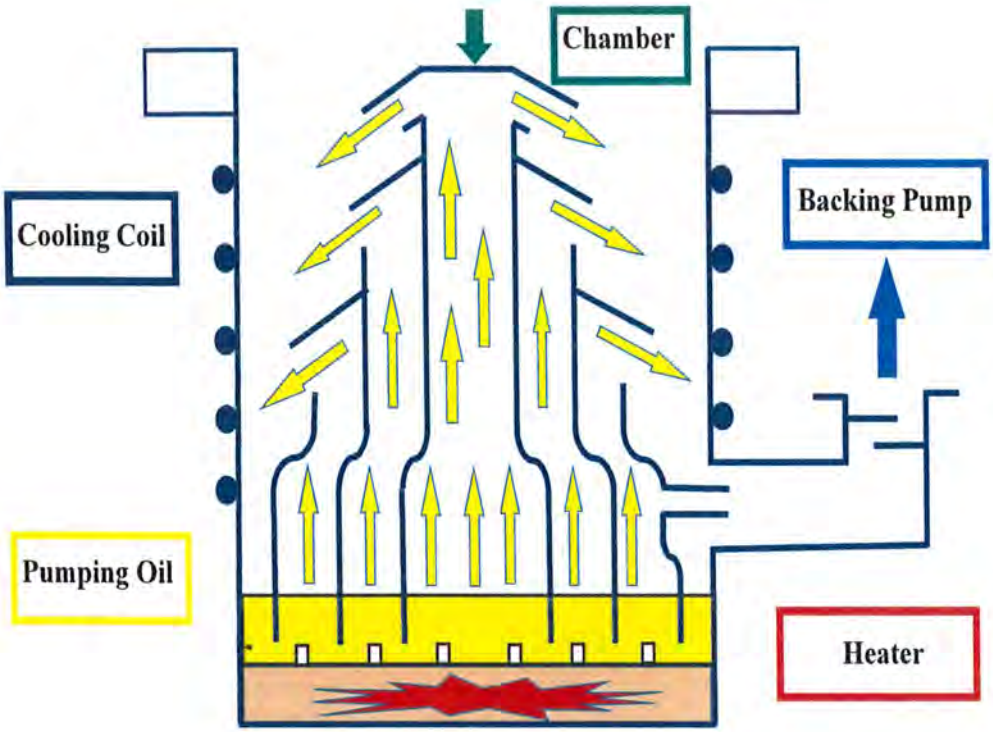

Figure 2.9: Typical Multistage Oil Diffusion Pump.

The ODP's effectiveness is influenced by numerous variables. The speed at which molecules enter the jet stream is governed by the molecular flow rate at the nozzle's axis. The dimensions of the stream, its speed, density, and the weight of the oil molecules inside it all influence how quickly air molecules diffuse into the jet and how much downward momentum increases. This can be seen by the fact that very few gas molecules will receive the extra momentum needed to compress the gas below the jet if the jet is not dense enough, and too many molecules will prevent gas molecules from diffusing into the jet if it is too dense. Jet characteristics are influenced by the nozzle shape, the oil's viscosity, and vapor pressure, as well as its sustainability at high working temperatures (usually 200°C). It is important to keep in mind that not all air molecules that diffuse into the jet are delivered to the exit; some of them contact with oil molecules and as a consequence, gas molecules go upward against the direction of flow. Consequently, we may argue that the probability of further propagation and collision is indeed smaller than one.

A significant disadvantage of ODP is backstreaming, where certain oil molecules begin to flow toward the sealed chamber after fleeing from the nozzle. If precautions are not taken, it will be possible

for oil molecules to pollute the surface of the chamber in comparatively minimal working time. Furthermore, Siliceous or Carbonaceous deposits may produce when it comes into interaction with electric discharges or heated filaments.

In the pump intake, baffles are positioned above the nozzle to diminish this impact. A typical chevron baffle layout is illustrated in Figure 2.10(a). It prevents oil molecules access to the chamber at all. As a result, they bump into it, get caught in the condensation and stored as a condensed liquid, trickle back into the pump, and eventually make their way back to the boiler. However, all of this comes with a 0.3-factor reduction in the conduction of gas molecules into the pump and the rate of the pump above the baffle. The insertion of a specifically made cap above is another approach that does not completely solve the issue but greatly decreases it. The nozzle system, also known as the cold cap, is illustrated in Figure 2.10. (b). It is maintained significantly colder by being connected to a water-cooled pump body, where it intercepts and condenses an oil molecule. Thus, the boiler receives 95% or more of the back-streaming flow.

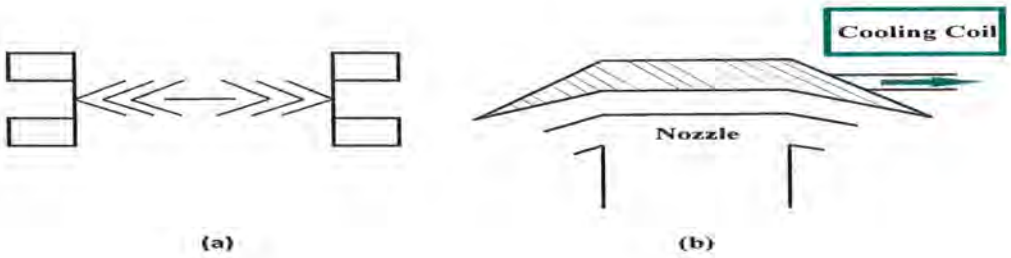

Figure 2.10: (a) Chevron Baffle, and (b) Cold Cap

2.3 Ion Detector

The function of an ion detector is the collection of ions that are generated in the plasma. The Langmuir Probe, which is illustrated in figure 2.11, is the most often used ion detector, which has probably a 5 mm diameter. It is an instrument utilized for plasma examinations that can measure the electron density, electron temperature, and other variables of plasma. It operates by introducing one or more electrodes into the plasma while maintaining a steady or time-varying electric potential between the electrodes or between them and the chamber. In our experiment, we used a homemade Langmuir probe ion detector.

The probe can be made from a thin metal rod i.e. aluminium. The length of the probe is about 10 mm while diameter of the probe tip is 0.38 mm. The probe should be mounted on a support, such as a ceramic rod, so that it can be easily positioned within the plasma. The support should also provide electrical insulation between the probe and the ground. We gather ion signals by providing a negative voltage to the probe and determine the various plasma characteristics by using measured potentials and currents.

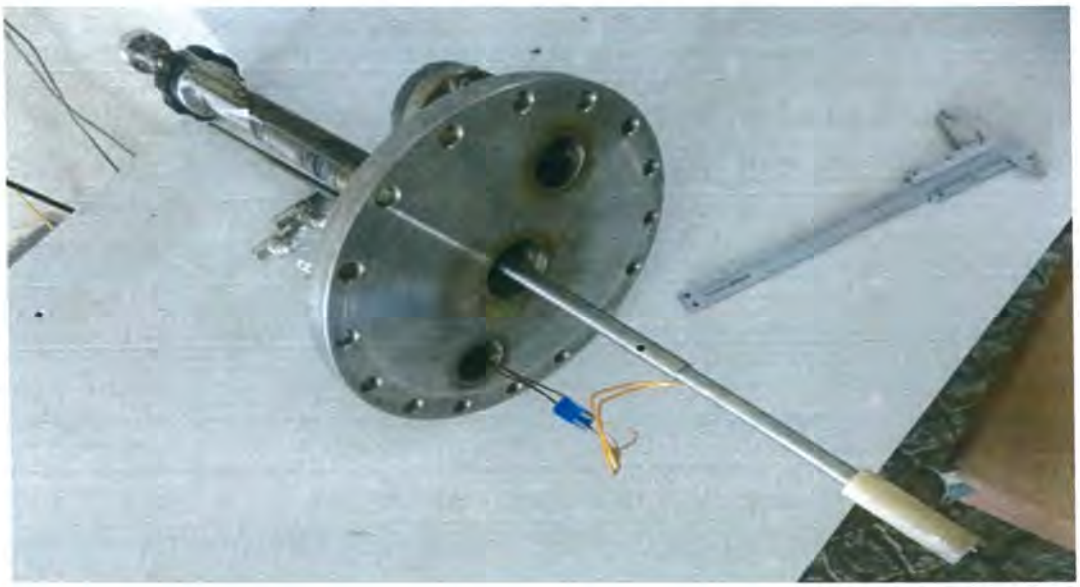

Figure 2.11: The Ion detector

2.4 Oscilloscope

An oscilloscope, commonly referred to as an oscillograph, is a device that graphically displays electrical signals and illustrates how these signals change over time. In our experiment, we have used Tektronix TDS-2024 (four-channel digital storage oscilloscope) with a frequency of 200 MHz and it is externally triggered. The common parts used in the digital storage oscilloscope are shown in the block diagram in Figure 2.12. The first part is an amplifier device that enables the magnitude of the input voltage signal to be adjusted to a suitable level. The input data is then sampled at defined points in time by an analog-to-digital converter. Before entering a microprocessor, the acquisition storage component stores the values of the sampled signals. This executes signal processing operations, controls front panel control settings, and sets up the output display. After that, a display memory module stores the output

signal before it is sent to the display. This comprises a liquid crystal display, which can be either monochrome or multicolored. Instead of appearing as a continuous line like an analogue oscilloscope would, the signal is really presented as a series of discrete dots. However, the picture gets more and more like a continuous line as the dot density rises. The sampling rate used to digitize the analogue signal and the reading rate used to reassemble the original signal's memory contents have a direct impact on the dot density.

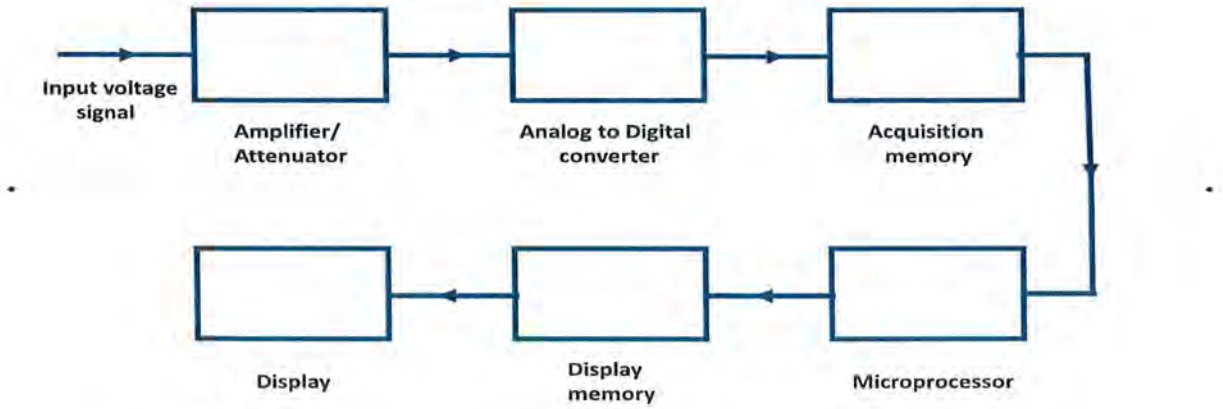

Figure 2.12: The block diagram of the common parts used in the digital storage oscilloscope.

Aside from exhibiting the amplitude of voltage signals, they can also showcase other factors such as phase and frequency. Furthermore, they have the capability to examine the waveform detected and calculate various signal traits including maximum and minimum signal levels, peak-peak values, mean values, rms values, as well as the rise and fall times.

CHAPTER 3

Results and Discussions

We have used the ion detector to examine the kinetic energy distributions and charge per pulse in order to explore the essential attributes of the ion emission from the laser-produced plasma. The time-of-flight ion spectra obtained from an Aluminium (Al) target using an ion detector are illustrated in Figure 3.1. The ion detector was positioned 4.5 cm away from the sample, perpendicular to the sample's surface. Measurements were taken at double pulse mode having a wavelength of 532 nm each while keeping the energy of the first laser is 34 mJ and the second laser is 62 mJ. Each curve shows the average ion signal obtained for different delays of double-pulse with single shots. The second laser pulse has quife diverse effects on the plasma that was produced by the pulse of the first laser relying on the inter-pulse delay. The second pulse increased the plasma average charge state and maximal ion kinetic energy at longer delays, it also strongly enhanced the production of low-charge ions (particularly single-charge ions) at longer delays while leaving the energies and rates of high charge unaffected.

Figure 3.2 displays t.o.f. data separately for each inter pulse delay from the same DP experiment performed on Aluminium targets that were produced using pulses with fluencies; 120.3 J/cm^2 for the plasma laser and 219.4 J/cm^2 for the probe laser, respectively. With the use of this laser fluence relation, we can examine the impact of a strong energy laser pulse on the plasma created by a low laser pulse. The signals are divided into two time-of-flight peaks with some delays between them. The lower t.o.f peaks does not change their t.o.f position for changing inter-pulse delay whereas the higher t.o.f. peak is inter-pulse delay-dependent and appears at 5.7 μs, 5.8 μs, 6 μs, 6.2 μs and 6.5 μs when the inter-pulse delay is 550 ns, 570 ns, 600 ns, 650 ns, and 750 ns respectively. In this instance, the intensity of the first peak at lower t.o.f values is almost independent of the duration between the pulses. They remain at the same amplitude value.

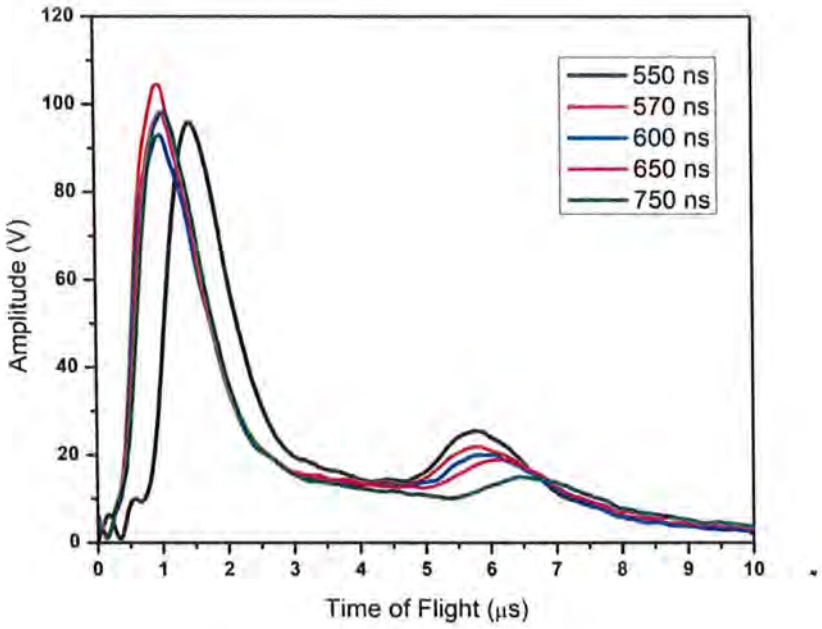

Figure 3.1: ion signal at laser fluence 120.3 J/cm² and 219.4 J/cm² for wavelength 532nm at different inter pulse time

However, the intensity of a second peak at higher t.o.f. values were sensitive to the inter-pulse delay, its amplitude decreases as we increase the delay time between the pulses. When the delay is greater than a few microseconds, signals appear that are consistent with the development of two distinct plasmas, the later plasma is created after a delay that is comparable to the delay at which the probe laser was fired.

The combined signals of double pulse and single pulse laser are mentioned in figure 3.3. A Single Pulse (SP) experiment with the plasma laser of fluency *219.4 J/cm²* was shifted to a small value of t.o.f scale while the probe laser of fluency 219.4 *J/cm²* (dashed black lines) was observed at the higher t.o.f value comparatively. However, the intensities and energy of these signals vary depending on the laser intensity. The peak intensity of the probe laser is greater than the plasma laser. SP signals have a large temporal range and peak at around -6.3 μs and -1.9 μs, respectively. The low-energy peak remained near 1.3 μs, registered by the plasma laser in SP experiments while the high-energy one was sensible to the inter-pulse delay.

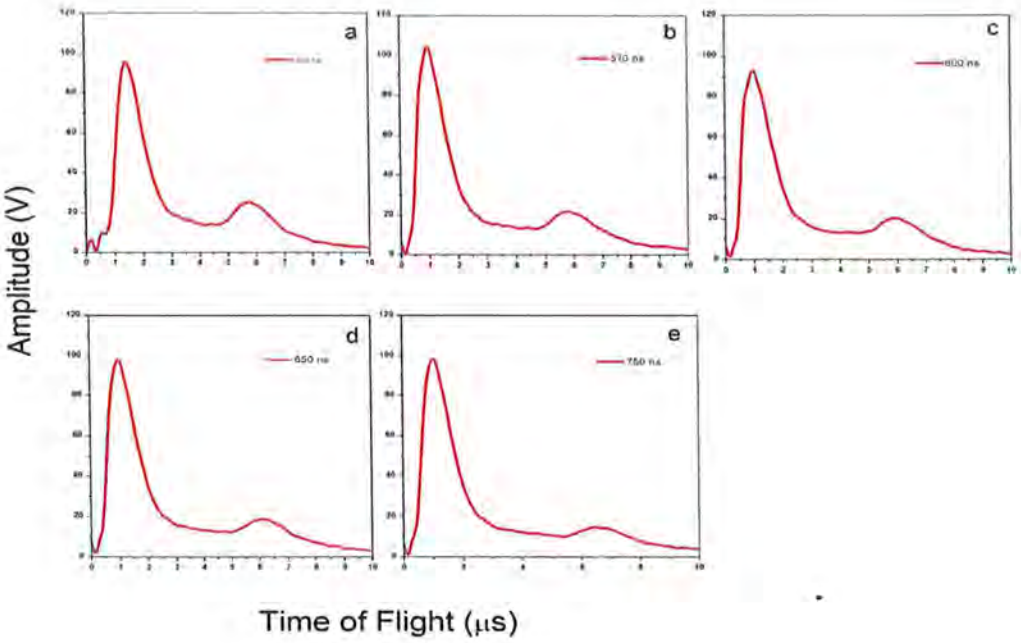

Figure 3.2: T.o.f. traces collected from the ion probe in DP experiments at delays of 550 ns (a), 570 ns (b), 600 ns (c), 650 ns and (d), 750 ns. Laser energies used to produce the plasma and to probe it were 120.3 J/cm² and 219.4 J/cm² J, respectively. The target was aluminum.

The combined signals of double pulse and single pulse laser are mentioned in figure 3.3. A Single Pulse (SP) experiment with the plasma laser of fluency *219.4 J/cm²* was shifted to a small value of t.o.f scale while the probe laser of fluency 219.4 *J/cm²* (dashed black lines) was observed at the higher t.o.f value comparatively. However, the intensities and energy of these signals vary depending on the laser intensity. The peak intensity of the probe laser is greater than the plasma laser. SP signals have a large temporal range and peak at around 3 μs and 3.6 μs, respectively. The low-energy peak remained near 1.3 μs, registered by the plasma laser in SP experiments while the high-energy one was sensible to the inter-pulse delay. The intensity of the low energy peak remains unchanged and no shift occurs with the increment of inter-pulse delay, while the intensity of the high energy peaks was decreasing and also their peaks are shifted to the higher t.o.f value as the delay between the pulse increases. The signals of the DP experiment were strongly displaced to a higher t.o.f. values and the positions of the peaks were discussed in figure 3.2.

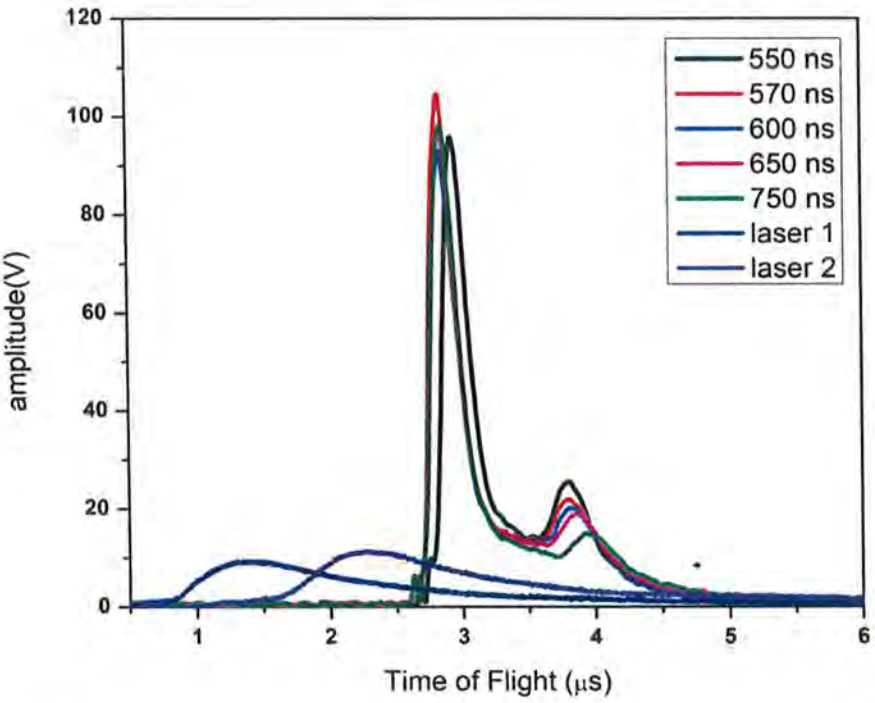

Figure 3.3: Combined ion signal of SP and DP at laser fluencies of 120.3 J/cm² and 219.4 J/cm² for wavelength 532nm at different inter-pulse time.

The average kinetic energy and total charge per pulse for the Aluminum (Al) ions are investigated from the figure 3.1. the average energy of the ions is calculated as;

$$< E >= \left(\frac{M}{2}\right)\left(d/_{< t >}\right)^2. \qquad (3.1)$$

Where M is the mass of Al ion, d is the distance between the sample's surface and ion detector, and average time < t > is given by

$$< t >= \frac{\int_{t_i}^{t_f} t \times V(t)dt}{\int_{t_i}^{t_f} V(t)dt}, \qquad (3.2)$$

where $V(t)$ is the voltage measured by the ion detector and t_i and t_f are the times that correspond to the beginning and end of the ion signal.

The average kinetic energy of the peaks for various inter-pulse delays is plotted in figure 3.4. the graph illustrates the comparison of the peak average energy of the plasma laser and the probe laser with

the inter-pulse delay. The probe laser's (the second laser which is used to heat up the plasma) peak average energy is plotted in graph 3.4 (a). The trend of this graph indicates that the energy decreases as we increase the inter-pulse delay. The decreasing trend is so smooth with delay. The plasma laser (The first laser which generates the plasma) peak energy is plotted next to the probe laser in figure 3.4 (b). The flow of this graph shows no dependence of the inter-pulse delay on the peak energy at all.

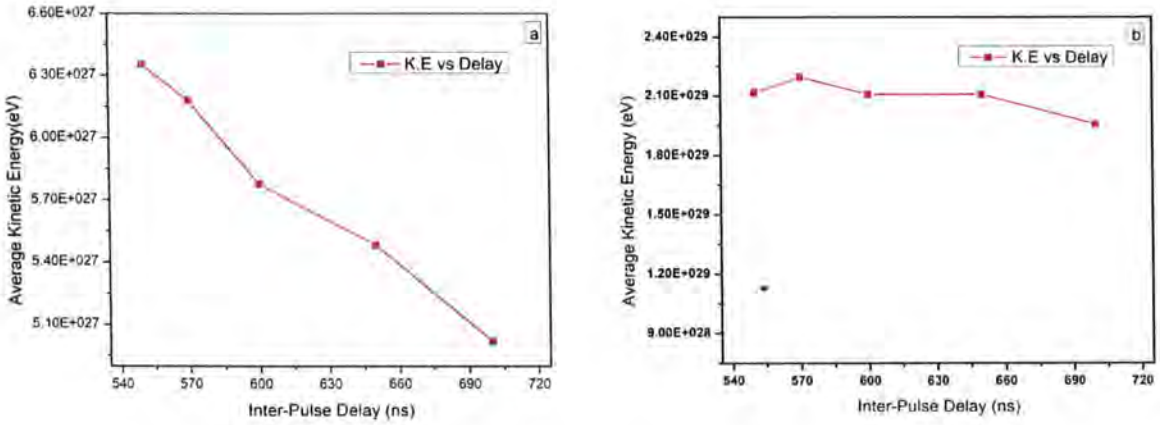

Figure 3.4: Kinetic energy of Al ions as a function of inter-pulse delay, K.E of plasma laser (a) and probe laser (b).

To study the effect of inter-pulse delay on ion's charge per pulse Q, we simply integrate the corresponding ion spectra shown in figure 3.5. As

$$\int_{t_i}^{t_f} V(t)dt = \int_{t_i}^{t_f} RI(t)dt = \int_{t_i}^{t_f} R\frac{dQ}{dt}dt\,, \tag{3.3}$$

$$R\int_{Q_i}^{Q_f} dQ = RQ, \tag{3.4}$$

$$Q = \frac{\int_{t_i}^{t_f} V(t)dt}{R}. \tag{3.5}$$

Where R is the resistance across which ion signal is measured, Q_i and Q_f are the charges at the start and end of the signal and $I(t)$ is the ion current at any given moment in time.

Figure 3.5 shows the ion charge per pulse calculated for five different inter-pulse. The trend of the charge per pulse for small peaks (i.e. the probe laser peaks shows in figure 3.5 (a)) with the inter pulse delay shows same behavior as kinetic energy of the peaks (i.e. like with the increase of inter-pulse

delay the charge per pule decreases). The decrease is due the fact that the peaks were going down in amplitude as delay enhanced which cause the decline in the peak K.E.

The trend of the large peaks (i.e. plasma laser peak) shows very strange pattern illustrated in figure 3.5 (b). The investigation indicates that the charge per pulse were at highest point at the smallest delay (i.e. 550 ns), but as the delay increased up to 600 ns, the charge goes to minimum value. After that as the delay further increased above 600 ns to 750 ns, the charge starts growing to increases.

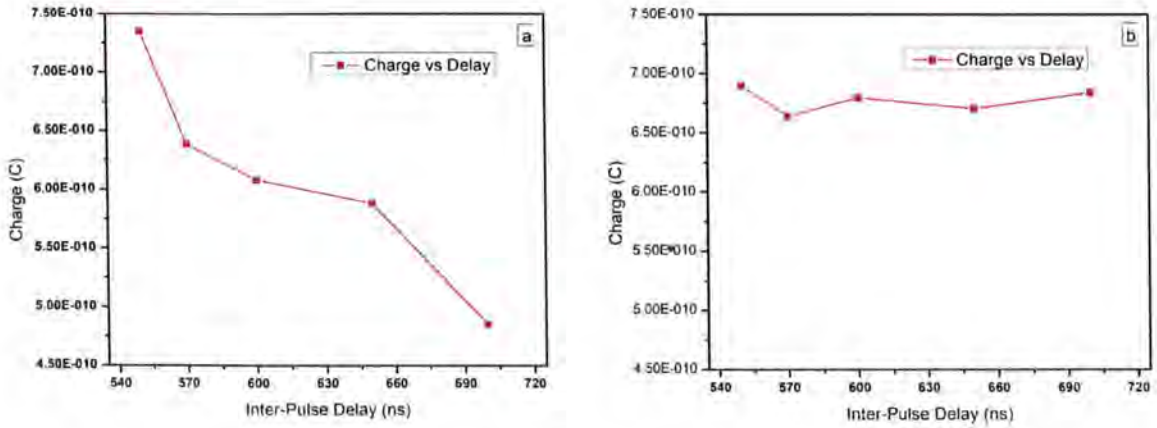

Figure 3.5: Ion charge as a function of inter-pulse time of plasma laser (a) and probe laser (b).

Figure 3.6 shows kinetic energy distributions(KED) and reveal the effect of inter-pulse delay on the kinetic energy distribution of ions produced from ablation of an Al target with double and single pulse lasers. The KEDs of the double pulse laser are shown in Figure 3.5(a) for different delays and Figures 3.5 (b) and (c) show the KEDs of the plasma laser and probe laser, respectively, in the single pulse mode. It is clear that the KEDs of the double pulse laser overlap in the lower energy region, but a noticeable difference can be seen in the higher energy range. Furthermore, the area of the KEDs for the plasma laser is narrower than that of the probe laser due to its lower laser fluence (120.3 J/cm2 compared to 219.4 J/cm2 for the probe laser). This dependence on the laser fluence suggests that it has a direct impact on the KEDs of the ion signals. The decay of ion intensity at high laser fluence is slower compared

to low laser fluence. The results also indicate that the double pulse laser has larger KEDs compared to the single pulse mode.

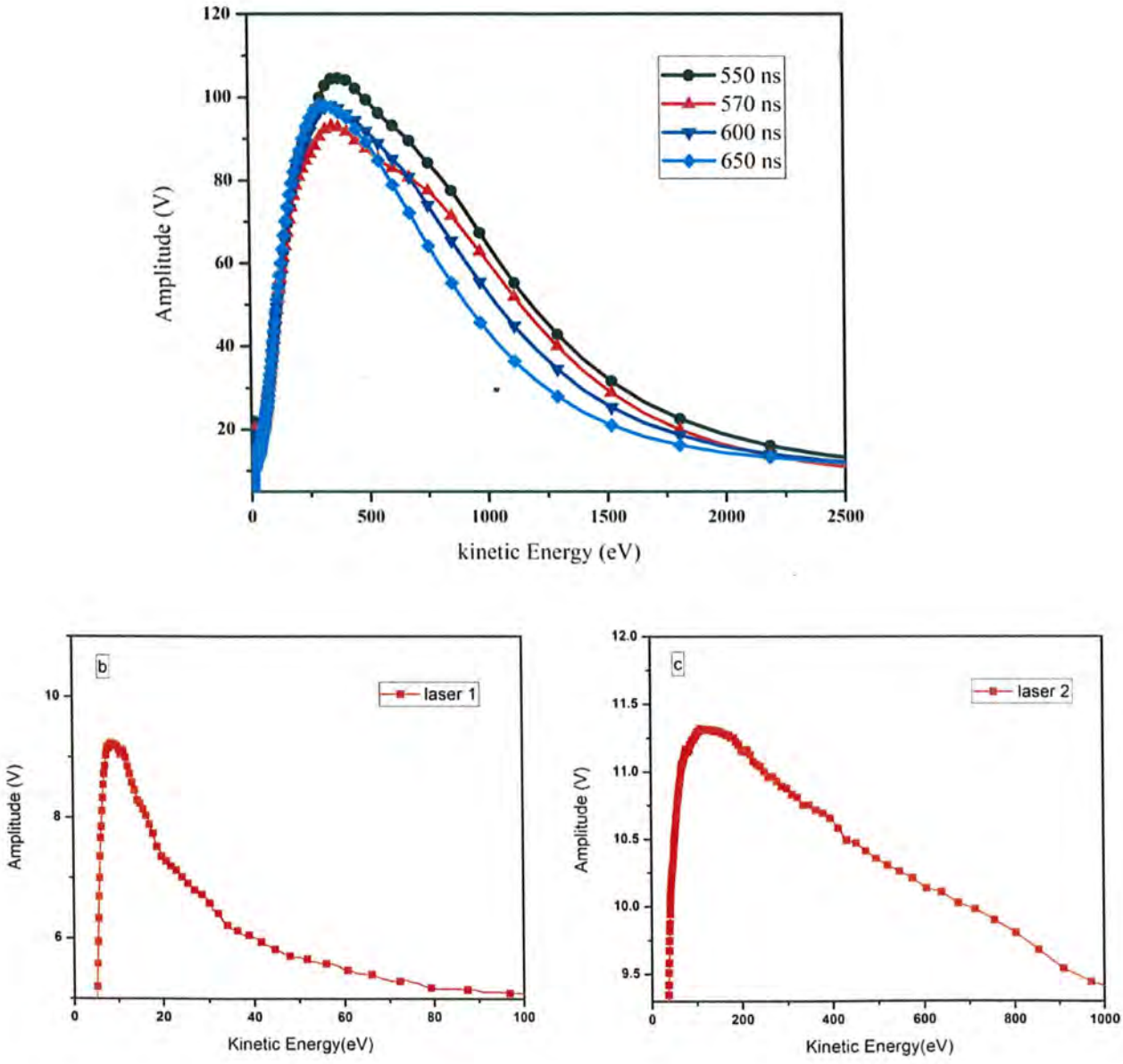

Figure 3.6: Kinetic Energy Distribution (KEDs) of ions for double pulse laser at delays of 550 ns, 570 ns, 600ns and 650sn (a), single pulse plasma laser (b), and probe laser (c)

CONCLUSION

In summary, we have investigated the coupling between laser produced plasmas and probe laser pulses at varying inter-pulse time in the nanosecond time scale. We examined the impact of inter-pulse timing on the creation of ions produced by laser-produced plasmas (LPP) in a vacuum. The calculations were performed to study the effects on average kinetic energy, kinetic energy distributions of Al ions and charges per laser pulse produced by a 532 nm Q-switched Nd:YAG laser. For studying effects of changing inter-pulse delay, we used second harmonic i.e., 532nm. The analysis was carried out in the specific range of inter-pulse delays i.e., 550 ns, 570 ns, 600 ns, 650 ns and 750 ns.

During this experiment, the initial stages will result in the creation of ions that rapidly expand. The remainder of the laser pulse will undergo screening and will partially be absorbed by the plasma core, particularly increasing the number of Al ions. A combination of a plasma produced by a laser with a second pulse can be utilized to assess the dynamics of plasma formation and growth in plasmas generated by lasers.

In our observed ion signal, we observe a sharp increase in the amplitude of ion current that rises to a maximum value and then decreases slowly but the delayed laser gives another peak which then decreases as the plume begins to expand beyond ion detector. Also, we observed that the lower t.o.f peaks does not change their t.o.f position for changing inter-pulse delay whereas the higher t.o.f. peak is inter-pulse delay-dependent and appears at 5.7 μs, 5.8 μs, 6 μs, 6.2 μs and 6.5 μs when the inter-pulse delay is 550 ns, 570 ns, 600 ns, 650 ns, and 750 ns respectively.

We calculated average ion energy and charge per pulse for each inter-pulse delay and observed that ions of plasma Laser have no dependence on inter-pulse delay and decreasing linear behavior was seen with increasing inter-pulse delay for the probe laser. Same trend was followed by the ion charge per pulse as a function of inter-pulse delay.

REFERENCES:

[1] F.F. Chen, Introduction to plasma physics and controlled fusion, Springer, 1984.

[2] R. Goldston, P. Rutherford, Introduction to Plasma Physics, Inst. of Phys, Publ., Bristol, (1995).

[3] E. Sharon, Black Laser Ablation: Effects and Applications, Nova, New York, (2011).

[4] R.K. Singh, J. Narayan, Pulsed-laser evaporation technique for deposition of thin films: Physics and theoretical model, Physical review B, 41 (1990) 8843.

[5] C. Phipps, Laser ablation and its applications, Springer, 2007.

[6] M. Stafe, I. Vladoiu, I.M. Popescu, Impact of the lasr wavelength and fluence on the ablation rate of aluminium, Central European Journal of Physics, 6 (2008) 327-331.

[7] M. Stafe, A. Marcu, N.N. Puscas, Laser-matter interaction below the plasma ignition threshold intensity, in: Pulsed Laser Ablation of Solids, Springer, 2014, pp. 53-76.

[8] S. Thakur, J. Singh, Fundamentals of laser induced breakdown spectroscopy, in: Laser-induced breakdown spectroscopy, Elsevier, 2007, pp. 3-21.

[9] C. Pasquini, J. Cortez, L. Silva, F.B. Gonzaga, Laser induced breakdown spectroscopy, Journal of the Brazilian Chemical Society, 18 (2007) 463-512.

[10] B. Stuart, M. Feit, A. Rubenchik, B. Shore, M. Perry, Laser-induced damage in dielectrics with nanosecond to subpicosecond pulses, Physical review letters, 74 (1995) 2248.

[11] J. Ihlemann, A. Scholl, H. Schmidt, B. Wolff-Rottke, Nanosecond and femtosecond excimer-laser ablation of oxide ceramics, Applied Physics A, 60 (1995) 411-417.

[12] B.N. Chichkov, C. Momma, S. Nolte, F. Von Alvensleben, A. Tünnermann, Femtosecond, picosecond and nanosecond laser ablation of solids, Applied physics A, 63 (1996) 109-115.

[13] J. Fujimoto, J. Liu, E. Ippen, N. Bloembergen, Femtosecond laser interaction with metallic tungsten and nonequilibrium electron and lattice temperatures, Physical Review Letters, 53 (1984) 1837.

[14] H. Elsayed-Ali, T. Norris, M. Pessot, G. Mourou, Time-resolved observation of electron-phonon relaxation in copper, Physical Review Letters, 58 (1987) 1212.

[15] R. Schoenlein, W. Lin, J. Fujimoto, G. Eesley, Femtosecond studies of nonequilibrium electronic processes in metals, Physical Review Letters, 58 (1987) 1680.

[16] S. Brorson, A. Kazeroonian, J. Moodera, D. Face, T. Cheng, E. Ippen, M. Dresselhaus, G. Dresselhaus, Femtosecond room-temperature measurement of the electron-phonon coupling constant γ in metallic superconductors, Physical Review Letters, 64 (1990) 2172.

[17] G. Eesley, Generation of nonequilibrium electron and lattice temperatures in copper by picosecond laser pulses, Physical Review B, 33 (1986) 2144.

[18] D. Bäuerle, Laser Processing and Chemistry, Springer, in, Berlin, 2000.

[19] M.v. Allmen, A. Blatter, Evaporation and plasma formation, in: Laser-beam interactions with materials, Springer, 1995, pp. 115-165.

[20] P. Haglund, I. Eriksson, J. Powell, A. Kaplan, Surface tension stabilized laser welding (donut laser welding)—A new laser welding technique, Journal of laser applications, 25 (2013) 031501.

[21] C. Draper, J. Poate, Laser surface alloying, International metals reviews, 30 (1985) 85-108.

[22] M. Stafe, C. Negutu, I. Vladoiu, A.N. Ducariu, I.M. Popescu, Experimental investigation of the dimensions and quality of laser-drilled holes in metals, in: Optical Manufacturing and Testing VIII, SPIE, 2009, pp. 307-314.

[23] M. Stafe, C. Negutu, A. Ducariu, Pulsed laser ablated craters on aluminum in gaseous and aqueous environments, Romanian Reports in Physics, 64 (2012) 155-162.

[24] M. Stafe, I. Vladoiu, C. Negutu, I.M. Popescu, Experimental investigation of the laser-drilled holes in aluminium, UPB Sci. Bull. Ser. A, 71 (2009) 73-80.

[25] C. Negutu, I. Vladoiu, M. Stafe, A. Rizea, N. Puscas, I. Popescu, Effect of pulse number on the ablation rate of metals in PLA multi-pulse regime, in: Advanced Topics in Optoelectronics, Microelectronics, and Nanotechnologies V, SPIE, 2010, pp. 134-139.

[26] P. Stavropoulos, C. Palagas, G. Angelopoulos, D. Papamantellos, S. Couris, Calibration measurements in laser-induced breakdown spectroscopy using nanosecond and picosecond lasers, Spectrochimica Acta Part B: Atomic Spectroscopy, 59 (2004) 1885-1892.

[27] G. Cristoforetti, E. Tognoni, L. Gizzi, Thermodynamic equilibrium states in laser-induced plasmas: From the general case to laser-induced breakdown spectroscopy plasmas, Spectrochimica Acta Part B: Atomic Spectroscopy, 90 (2013) 1-22.

[28] G. Cristoforetti, G. Lorenzetti, S. Legnaioli, V. Palleschi, Investigation on the role of air in the dynamical evolution and thermodynamic state of a laser-induced aluminium plasma by spatial-and time-resolved spectroscopy, Spectrochimica Acta Part B: Atomic Spectroscopy, 65 (2010) 787-796.

[29] B. Wolf, Handbook of ion sources, CRC press, 1995.

[30] R.O. Dendy, Plasma physics: an introductory course, Cambridge University Press, 1995.

[31] A. Galmed, M. Harith, Temporal follow up of the LTE conditions in aluminum laser induced plasma at different laser energies, Applied Physics B, 91 (2008) 651-660.

[32] J.B. Simeonsson, A. Miziolek, Spectroscopic studies of laser-produced plasmas formed in CO and CO2 using 193, 266, 355, 532 and 1064 nm laser radiation, Applied Physics B, 59 (1994) 1-9.

[33] H.R. Griem, Validity of local thermal equilibrium in plasma spectroscopy, Physical Review, 131 (1963) 1170.

[34] G. Cristoforetti, A. De Giacomo, M. Dell'Aglio, S. Legnaioli, E. Tognoni, V. Palleschi, N. Omenetto, Local thermodynamic equilibrium in laser-induced breakdown spectroscopy: beyond the McWhirter criterion, Spectrochimica Acta Part B: Atomic Spectroscopy, 65 (2010) 86-95.

[35] J.A. Bittencourt, Fundamentals of plasma physics, Springer Science & Business Media, 2004.

[36] M. Sabsabi, P. Cielo, Quantitative analysis of aluminum alloys by laser-induced breakdown spectroscopy and plasma characterization, Applied Spectroscopy, 49 (1995) 499-507.

[37] R.A. Multari, L.E. Foster, D.A. Cremers, M.J. Ferris, Effect of sampling geometry on elemental emissions in laser-induced breakdown spectroscopy, Applied Spectroscopy, 50 (1996) 1483-1499.

[38] D. Rusak, B. Castle, B. Smith, J. Winefordner, Excitational, vibrational, and rotational temperatures in Nd: YAG and XeCl laser-induced plasmas, Spectrochimica Acta Part B: Atomic Spectroscopy, 52 (1997) 1929-1935.

[39] N. Shaikh, S. Hafeez, B. Rashid, M. Baig, Spectroscopic studies of laser induced aluminum plasma using fundamental, second and third harmonics of a Nd: YAG laser, The European Physical Journal D, 44 (2007) 371-379.

[40] N.M. Shaikh, S. Hafeez, M. Kalyar, R. Ali, M. Baig, Spectroscopic characterization of laser ablation brass plasma, Journal of applied physics, 104 (2008) 103108.

[41] J. Hoffman, T. Moscicki, Z. Szymanski, The effect of laser wavelength on heating of ablated carbon plume, Applied Physics A, 104 (2011) 815-819.

[42] N. Farid, C. Li, H. Wang, H. Ding, Laser-induced breakdown spectroscopic characterization of tungsten plasma using the first, second, and third harmonics of an Nd: YAG laser, Journal of nuclear materials, 433 (2013) 80-85.

[43] N.M. Shaikh, M. Kalhoro, A. Hussain, M. Baig, Spectroscopic study of a lead plasma produced by the 1064 nm, 532 nm and 355 nm of a Nd: YAG laser, Spectrochimica Acta Part B: Atomic Spectroscopy, 88 (2013) 198-202.

[44] N.M. Shaikh, Y. Tao, R. Burdt, S. Yuspeh, N. Amin, M. Tillack, Spectroscopic analysis of temperature and density of Sn plasma produced by a CO 2 laser, Journal of Applied Physics, 108 (2010) 083109.

[45] B. Le Drogoff, J. Margot, M. Chaker, M. Sabsabi, O. Barthelemy, T. Johnston, S. Laville, F. Vidal, Y. Von Kaenel, Temporal characterization of femtosecond laser pulses induced plasma for spectrochemical analysis of aluminum alloys, Spectrochimica acta part B: Atomic spectroscopy, 56 (2001) 987-1002.

[46] S. Laville, F. Vidal, T. Johnston, M. Chaker, B. Le Drogoff, O. Barthelemy, J. Margot, M. Sabsabi, Modeling the time evolution of laser-induced plasmas for various pulse durations and fluences, Physics of Plasmas, 11 (2004) 2182-2190.

[47] A. Elhassan, A. Giakoumaki, D. Anglos, G. Ingo, L. Robbiola, M. Harith, Nanosecond and femtosecond laser induced breakdown spectroscopic analysis of bronze alloys, Spectrochimica Acta Part B: Atomic Spectroscopy, 63 (2008) 504-511.

[48] A. Sarkar, R.V. Shah, D. Alamelu, S.K. Aggarwal, Studies on the ns-IR-laser-induced plasma parameters in the vanadium oxide, Journal of Atomic and Molecular Physics, 2011 (2011).

[49] S. Harilal, C. Bindhu, V. Nampoori, C. Vallabhan, Temporal and spatial behavior of electron density and temperature in a laser-produced plasma from YBa2Cu3O7, Applied spectroscopy, 52 (1998) 449-455.

[50] L. Wu, R. Shen, J. Xu, Y. Ye, Y. Hu, Spectroscopic study of laser-induced cu plasma with and without the confinement of a substrate, IEEE transactions on plasma science, 38 (2010) 174-180.

[51] A.A. Khalil, A comparative spectroscopic study of single and dual pulse laser produced UV tin plasmas, Optics & Laser Technology, 45 (2013) 443-452.

[52] V. Pinon, D. Anglos, Optical emission studies of plasma induced by single and double femtosecond laser pulses, Spectrochimica Acta Part B: Atomic Spectroscopy, 64 (2009) 950-960.

[53] R. Sattmann, V. Sturm, R. Noll, Laser-induced breakdown spectroscopy of steel samples using multiple Q-switch Nd: YAG laser pulses, Journal of Physics D: Applied Physics, 28 (1995) 2181.

[54] G. Cristoforetti, S. Legnaioli, L. Pardini, V. Palleschi, A. Salvetti, E. Tognoni, Spectroscopic and shadowgraphic analysis of laser induced plasmas in the orthogonal double pulse pre-ablation configuration, Spectrochimica Acta Part B: Atomic Spectroscopy, 61 (2006) 340-350.

[55] P.A. Benedetti, G. Cristoforetti, S. Legnaioli, V. Palleschi, L. Pardini, A. Salvetti, E. Tognoni, Effect of laser pulse energies in laser induced breakdown spectroscopy in double-pulse configuration, Spectrochimica Acta Part B: Atomic Spectroscopy, 60 (2005) 1392-1401.

[56] P. Willmott, J. Huber, Pulsed laser vaporization and deposition, Reviews of Modern Physics, 72 (2000) 315.

[57] S. Amoruso, A. Amodeo, V. Berardi, R. Bruzzese, N. Spinelli, R. Velotta, Laser produced plasmas in high fluence ablation of metallic surfaces probed by time-of-flight mass spectrometry, Applied surface science, 96 (1996) 175-180.

[58] S. Amoruso, M. Armenante, V. Berardi, R. Bruzzese, N. Spinelli, Absorption and saturation mechanisms in aluminium laser ablated plasmas, Applied Physics A, 65 (1997) 265-271.

[59] Y.B. Zel'Dovich, Y.P. Raizer, Physics of shock waves and high-temperature hydrodynamic phenomena, Courier Corporation, 2002.

[60] X. Wang, S. Zhang, X. Cheng, E. Zhu, W. Hang, B. Huang, Ion kinetic energy distributions in laser-induced plasma, Spectrochimica Acta Part B: Atomic Spectroscopy, 99 (2014) 101-114.

[61] J.I. Apinaniz, F.J. Gordillo-Vázquez, R. Martínez, Ion energy distributions in laser-produced plasmas with two collinear pulses, Plasma Sources Science and Technology, 21 (2012) 015016.

[62] L. Torrisi, S. Gammino, Method for the calculation of electrical field in laser-generated plasma for ion stream production, Review of scientific instruments, 77 (2006) 03B707.

[63] L. Torrisi, S. Gammino, L. Andò, L. Laska, Tantalum ions produced by 1064 nm pulsed laser irradiation, Journal of applied physics, 91 (2002) 4685-4692.

[64] B. Toftmann, J. Schou, S. Canulescu, Energy distribution of ions produced by laser ablation of silver in vacuum, Applied surface science, 278 (2013) 273-277.

[65] W. Demtroder, W. Jantz, Investigation of laser-produced plasmas from metal-surfaces, Plasma Physics, 12 (1970) 691.